

AD704896

PRELIMINARY EVALUATION OF THE KERR EFFECT PHASE SHIFT AS A TECHNIQUE FOR CHEMICAL ANALYSIS

John R. Rowlands
Robert E. Linder
Eugene T. Krasicki

Southwest Research Institute

TECHNICAL REPORT AFAPL-TR-70-4

March 1970

This document has been approved for public release and sale,
its distribution is unlimited.

Air Force Aero Propulsion Laboratory
Air Force Systems Command
Wright-Patterson Air Force Base, Ohio

Reproduced by the
CLEARINGHOUSE
for Federal Scientific & Technical
Information Springfield Va. 22151

58

NOTICES

When Government drawings, specifications, or other data are used for any purpose other than in connection with a definitely related Government procurement operation, the United States Government thereby incurs no responsibility nor any obligation whatsoever; and the fact that the Government may have formulated, furnished, or in any way supplied the said drawings, specifications, or other data, is not to be regarded by implication or otherwise as in any manner licensing the holder or any other person or corporation, or conveying any rights or permission to manufacture, use, or sell any patented invention that may in any way be related thereto.

This document has been approved for public release and sale, its distribution is unlimited.

Copies of this report should not be returned unless return is requested by security considerations, contractual obligations, or notice on a specific document.



AFAPL-TR-70-1

PRELIMINARY EVALUATION OF THE KERR EFFECT PHASE SHIFT AS A TECHNIQUE FOR CHEMICAL ANALYSIS

John R. Rowlands

Robert E. Linder

Eugene T. Krasicki

This document has been approved for public release and sale,
its distribution is unlimited.

FOREWORD

This report was prepared by Southwest Research Institute, San Antonio, Texas, under Contract F33615-69-C-1231. The work reported herein was initiated under Project No. 3048, Task No. 304805. The work was performed by contractor's personnel using Air Force facilities at Wright-Patterson AFB. The program was administered by the Fuel Branch of the Fuels, Lubrication, and Hazards Division, Air Force Aero Propulsion Laboratory, Air Force Systems Command, Wright-Patterson AFB, Ohio. The Air Force project engineer is Mr. W. Melvyn Roquemore (APFF).

This technical report covers work performed between 2 December 1968 and 1 November 1969 under one phase of the subject contract. This report was submitted by the authors on 1 December 1969. Contractor's identifying numbers are Project No. 12-2497 and Report No. RS-536.

This technical report has been reviewed and is approved.



Arthur V. Churchill, Chief
Fuel Branch
Fuels, Lubrication, and Hazards Division
Air Force Aero Propulsion Laboratory

ABSTRACT

Several optical techniques are of interest as possible approaches to the chemical analysis of fuels and lubricants. Of these techniques, measurement of the phase shift or time lag in the Kerr effect was chosen for initial investigation. A breadboard device was constructed to measure the phase shift at frequencies from 200 Hz to 100 kHz. This device was used to measure the critical frequencies of poly- γ -benzyl-L-glutamate (1500 Hz), Acryloid HF-866 (1900 Hz), a probable impurity in lubricant ester S-9 (1000 Hz), and lubricant ester S-7 (>5 kHz), and also to analyze quantitatively a mixture of Acryloid HF-866 and the impure ester S-9. A spectrometer of simpler construction than the current instrument was designed to facilitate extending the measurements to higher frequencies on the order of 1 MHz, so that a wider range of molecular sizes and structures can be investigated. Also, the equations describing the Kerr response curve of mixtures were derived. Some numerical tests of the simple analysis procedures were compared with the results of these equations, and intensity and derivative spectra for representative mixtures were obtained.

TABLE OF CONTENTS

	<u>Page</u>
LIST OF ILLUSTRATIONS	vi
LIST OF TABLES	vii
I. INTRODUCTION	1
II. BASIS OF TIME LAGS	2
III. EXPERIMENTAL RESULTS AND INTERPRETATION	4
1. Apparatus	4
2. Results	5
IV. THEORETICAL MIXTURE ANALYSIS	8
V. SUMMARY	20
APPENDIXES	
I. Signal Shape Analysis	21
II. Theoretical Basis of Time Lags	23
III. Experimental Considerations	25
IV. Derivation of the Mixture Equations	31
V. Computer Program for Numerical Evaluation of Mixture Equations	35
VI. Differential Kerr Spectrometer	41
VII. Study of the Relaxation Time of the Kerr Effect by Alternating Current	43
VIII. Bibliography	51

LIST OF ILLUSTRATIONS

<u>Figure</u>		<u>Page</u>
1	D. C. Kerr Effect	2
2	Block Diagram of Apparatus	2
3	Kerr Frequency Response Curve	3
4	Electrical Schematic	4
5	Poly- γ -Benzyl-L-Glutamate Kerr Response Curve	6
6	Acryloid HF-866 Kerr Response Curve	6
7	Ester S-9 Kerr Response Curve	7
8	Mixture Kerr Response Curves	7
9	One-Component Kerr Response Curve	9
10	One-Component Kerr Response Curve	9
11	One-Component Kerr Response Curve	9
12	Two-Component Kerr Response Curves	10
13	Two-Component Kerr Response Curves	11
14	Two-Component Kerr Response Curves	12
15	Three-Component Kerr Response Curves	13
16	Three-Component Kerr Response Curves	14
17	Three-Component Kerr Response Curves	15
18	Three-Component Kerr Response Curves	16
19	One-Component Kerr Response Curve	17
20	One-Component Kerr Response Curve	17
21	Two-Component Kerr Response Curve	17
22	Electrical Analogy of the Kerr System	25
23	A Simple R-L-C Circuit	25
24	Resonance Current Curves for a Series R-L-C Circuit	30
25	Kerr Response Curve and Its Derivative with Respect to Frequency	41
26	Block Diagram of Differential Kerr Spectrometer	41

LIST OF TABLES

<u>Tables</u>		<u>Page</u>
I	Analysis of Mixture Response Curves	7
II	Summary of Parameters Used to Generate Figures 9 through 21	8
III	Simple Additivity Rules for Moderate Frequency Resolution	18
IV	Simple Additivity Rules for Poor Frequency Resolution	19
V	Modulation Parameters	22

BLANK PAGE

SECTION I

INTRODUCTION

The analysis of fuels and lubricants entails the resolution of complex mixtures and often the determination of materials present in trace quantities. A wide variety of conventional and instrumental techniques have been brought to bear on these problems, and satisfactory methods have been developed for many specific materials. However, there are many unsolved problems in this general field, and the development of new techniques is of definite interest.

Among the optical methods that have received scant attention, one may list those based on the Faraday effect, the Kerr effect, and fluorescence or phosphorescence spectra.

The work reported herein is the first phase of an investigation of time lags in the Kerr effect as a possible means of characterizing molecular size and structure.

SECTION II

BASIS OF TIME LAGS

When an electric field is applied to various substances, the material becomes doubly refracting. That is, the index of refraction for light polarized parallel to the field is different from that for perpendicularly polarized light. When the incident light is linearly polarized at 45 degrees to the electric field, the difference in indices of refraction leads to a phase shift between the components of the incident light polarization vector which are parallel and perpendicular to the applied electric field. The net result is that light emitted from the cell is now elliptically polarized rather than linearly polarized. This process is illustrated in Figure 1. The magnitude of the Kerr effect is described by

$$\Delta = \frac{1}{2} K F^2 \lambda \quad (1)$$

where Δ is the optical path difference between the parallel and perpendicular components; K , the Kerr constant, is defined by this relation; ℓ is the path length in the medium; F is the electric field strength; and λ is the wavelength of the incident light. Figure 2 shows the experimental arrangement. In block diagram form, as well as the qualitative shapes of the applied voltage and observed signal. In the experiment, the polarizer and analyzer are crossed so that no light is passed when the electric field is zero. When the electric field is applied, the light coming from the Kerr cell becomes elliptically polarized and, hence, some light is passed through the analyzer. This light is detected and the resultant voltage is amplified to give the observed

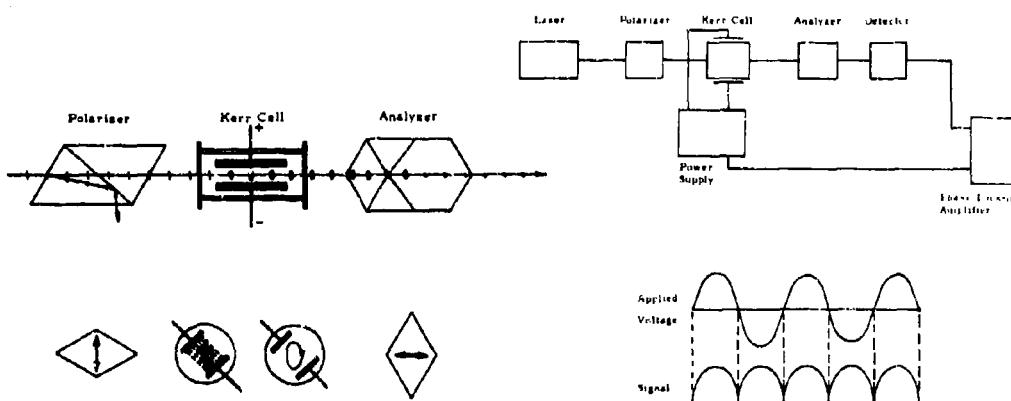


FIGURE 1. D. C. KERR EFFECT

FIGURE 2. BLOCK DIAGRAM OF APPARATUS

signal. An alternating field applied to the sample gives rise to a repetitive signal which has a characteristic shape. This shape may be used in the Lissajou pattern to determine the phase relationship of applied voltage and signal, or it may be analyzed in a phasemeter or lock-in amplifier to give the phase relationship directly. The function of a phase lock-in amplifier is to measure a certain frequency component of the input signal. It performs this function by comparing the input signal with a reference signal and amplifying that portion of the input signal that is in phase with the reference. In the present experiment, the reference signal was at the doubled frequency 2ω , for reasons given in Appendix I. This appendix contains the mathematical analysis of the frequency distribution of the light intensity signal.

From a molecular point of view, the Kerr effect has several origins. A molecule with an electric dipole moment tends to align itself with the electric field. The anisotropy of the medium thus produced causes the difference in indices of refraction and, hence, the Kerr effect. The fact that the molecule itself must be

oriented in this case indicates that finite times are involved. That is, the moment of inertia and interaction of the molecule with solvent molecules set a limit on the time it takes the molecule to align itself with the field. For a mathematical expression of the problem and the relationship of the response time of the molecule to molecular parameters, see Appendix II. This behavior manifests itself experimentally as a phase shift of the Kerr signal with respect to the applied voltage as well as an amplitude change in the signal. A qualitative explanation of this behavior is as follows. At low frequencies of the applied field, the molecules have ample time to align themselves with the field and, hence, stay almost in phase with it. At high frequencies, the molecules no longer have time to orient themselves and, hence, no orientation-based Kerr effect is measured. This behavior is illustrated in Figure 3, showing the Kerr constant and relative phase of applied field and signal as a function of frequency of the applied field.

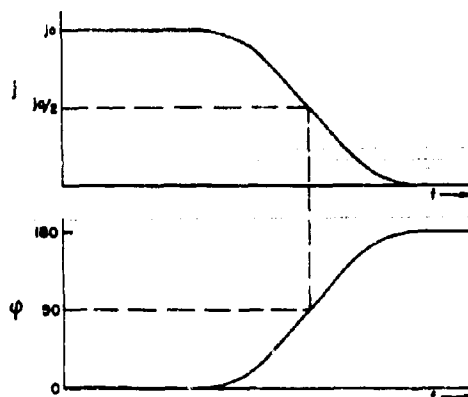


FIGURE 3. KERR FREQUENCY RESPONSE CURVE
(Permanent Moment)

A similar orientation behavior can be obtained if the electronic polarizability is anisotropic. In this case, the induced electric dipole moment has a preferential direction in the molecule. The molecule then tends to orient itself with the direction of maximum polarizability along the electric field direction. Since the same limits apply to the actual motion of the molecule, there are no differences in the theory for the rotational diffusion time (half amplitude point in Figure 3). However, the amplitude and phase curves are different from the permanent dipole case (see Appendix II). In this case, the Kerr signal goes to 90 degrees out of phase with respect to the driving voltage, as contrasted to the permanent dipole case where the limit is 180 degrees. Also, the amplitude goes to one-half its d.c. value instead of zero, as in the permanent dipole case.

In order to measure the molecular orientation phenomena, the frequency of the applied electric field is varied and the phase and amplitude of the observed signal is measured. These data are then collected in the form of a graph in which frequency is the x-axis and phase or amplitude is the y-axis. Determination of the shape of this curve then allows distinction between polar and nonpolar molecules, some estimation of degree of aromaticity, and determination of a geometry factor.

SECTION III

EXPERIMENTAL RESULTS AND INTERPRETATION

1. Apparatus

The Kerr cell electrodes were two parallel copper plates coated with gold and separated one from the other by a fixed distance d . The separation of the plates was made only large enough to permit the laser beam to pass between the plates without being depolarized. This distance d for the Kerr cell was approximately 0.118 in., i.e., slightly larger than the laser beam's diameter. The capacitance of a parallel-plate capacitor is

$$C = \frac{Q}{V_c} = \epsilon_o \epsilon_r \frac{A}{d} \text{ (farad)} \quad (2)$$

where

A is the area of the dielectric facing the electric flux lines expressed in square meters

d is the separation of the conductors expressed in meters

ϵ_r is the dielectric permittivity of the dielectric

$$\epsilon_o = \frac{1}{36\pi \times 10^9} \frac{F}{m} \text{ permittivity of free space}$$

By use of Equation (2), one can determine the capacitance of the Kerr cell by its dimensions and the dielectric constants of the material being examined between the plates of the Kerr cell. The capacitance of the Kerr cell varied from 10 to 100 pF in the experiments performed.

An electrical schematic of the apparatus is shown in Figure 4. The optical components are given for reference only, the actual optical system being as in Figure 2. The system, as represented here, was operated as a tuned R-L-C circuit (see Appendix III) for the purpose of achieving maximum voltage across the Kerr cell with minimum input power. Voltages of 20 kV, peak to peak at frequencies up to 100 kHz, were achieved.

The Kerr signal produced by this voltage was checked for authenticity in the following way. First, the laser beam was cut off by a piece of cardboard. The disappearance of the signal when this was done showed that the Kerr signal was not caused by electronic pickup or by ground loops in the apparatus. Also, a rotation of the polarizers by 90 degrees caused the Kerr signal to invert, as is proper. It was therefore concluded that the signal observed was truly a result of the normal Kerr effect.

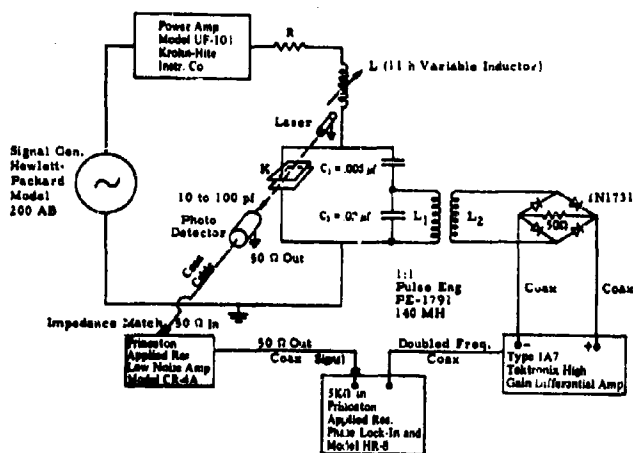


FIGURE 4. ELECTRICAL SCHEMATIC

The apparatus was used in the following manner:

- (1) The R-L-C circuit parameters were set for a resonant frequency in the range required.
- (2) The signal generator was tuned to the resonant frequency by maximizing the voltage across the Kerr cell, which was set to the level required.
- (3) The signal was then observed on the lock-in amplifier. (This signal was at twice the original frequency because the Kerr effect signal is proportional to $\sin^2\theta$. See Appendix I for an analysis of the amplitude of the Kerr signal at the doubled frequency.)
- (4) The phase measurements were performed by finding the phase at which the reference signal from the lock-in amplifier and the input signal (Kerr signal) were 90 degrees out of phase, i.e., the null point. The null point was verified for weak signals by finding the point at which blocking the laser beam caused no shift in the meter deflection. A further check on the null was made, in some cases, by disconnecting the Kerr cell leads and operating the system as if it were connected. This procedure determines the extent of electrical pickup, for which the data can then be corrected. The data, therefore, contain no error due to electrical pickup.
- (5) The amplitude of the Kerr signal was measured by changing the reference phase with respect to the input phase by 90 degrees and noting the deflection of the lock-in meter. The measured Kerr signal was the difference between the in-phase deflection and the null deflection, thus canceling pickup deflections.
- (6) The procedure was repeated at each frequency until the pertinent range was covered.
- (7) The procedure was repeated with the nitrobenzene Kerr cell in place to provide data for canceling apparatus phase shifts and amplitude changes as a function of frequency.

2. Results

The experiments performed so far have had several purposes. In the first experiments, poly- γ -benzyl-L-glutamate (PBLG) was used to check out the equipment and methods. PBLG is a polypeptide which can exist in the form of an α -helix, leading to a vector addition of monomer dipole moments and a large total electric dipole moment. Its high molecular weight (between 200,000 and 400,000 for our sample) and large dipole moment make this compound an ideal one on which to test the method. The phase and amplitude curves were obtained by comparison with similar curves for nitrobenzene. This normalization was made necessary because of phase and gain changes in the electronic equipment with changes in frequency. In this normalization procedure, nitrobenzene was made the reference material, assuming that no phase shift or amplitude change should have been observed for this compound. Thus, the raw data for PBLG were treated in the following ways:

- (1) At a given frequency, the measured phase shift of the nitrobenzene was subtracted from the PBLG phase shift to give the relative phase shift between the two compounds. Equipment phase shifts are thus subtracted out.
- (2) The amplitude of the PBLG signal at each frequency was scaled up by the ratio of the amplitude of the nitrobenzene at the lowest frequency used to that at the frequency in question. This essentially returns the gain to that of the lowest frequency measured.

Figure 3 shows the normalized curve obtained for PBLG. Our sample was found to have its 90-degree phase point (approximately the critical frequency) at about 1500 Hz.

The next set of experiments was performed on compounds of interest to the Air Force and were supplied by them. One was an oil additive used to improve viscosity-temperature properties, known as

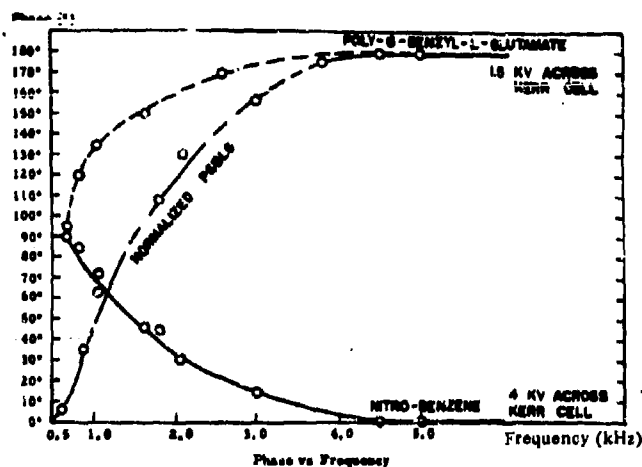


FIGURE 5. POLY- γ -BENZYL-L-GLUTAMATE KERR RESPONSE CURVE

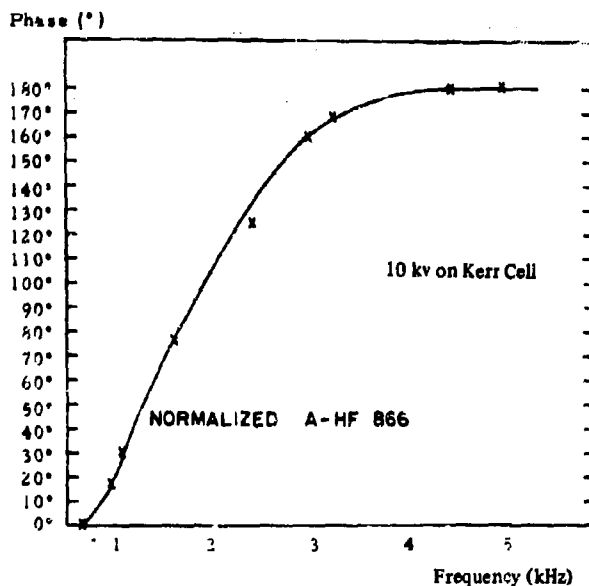


FIGURE 6. ACRYLOID HF-866 KERR RESPONSE CURVE

Acryloid HF-866. Its molecular weight is of the order of 10^5 . The experiment was performed to show the feasibility of further experiments designed to measure geometry changes in the Acryloid with temperature variations, and thus develop a method of evaluating the effectiveness of other additives of this nature. The preliminary experiments were successful, showing a critical frequency for this compound of approximately 1900 Hz. The normalized data are given in Figure 6.

Additional time and equipment will be necessary to measure this critical frequency as a function of temperature and, hence, measure the geometry change in the molecule. Incidental information gathered from this experiment includes the fact that the Acryloid has a permanent dipole moment as indicated by the phase curve going to 180 degrees.

Another compound studied in this phase was an ester known as S-9, used as a base stock for synthetic lubricants. This compound has a molecular weight of about 555, which makes the data obtained from it (shown in Figure 7) very difficult to understand. The critical frequency for this sample was measured to be about 1000 Hz—very low for a molecule of this size. A gross estimate of its expected critical frequency gave 100 MHz. Accordingly, the measurements on S-9 were repeated, and the data were found to be in error. These measurements showed no phase shift with respect to nitrobenzene for ester S-9 in the frequency region studied (1 kHz - 100 kHz). The data first obtained are presumed to be caused by small amounts of polypeptide remaining from previous tests.

Experiments on a similar ester, known as S-7, show the expected response. The data are not reported, because no phase shift or amplitude change with respect to nitrobenzene was measured. This is the proper behavior for a compound with a very high critical frequency. These data lend support to the impurity explanation of the S-9 data, since S-7 and S-9 are very similar in molecular structure.

The final series of experiments was performed to show the feasibility of analyzing mixtures using the phase method. In this work, the ester S-9 and Acryloid HF-866 were mixed to give approximately equal

contributions to the Kerr response curve (Figure 8). The response curve of the mixture was measured and the phase curve was analyzed according to the equations

$$\phi_T = f_A \phi_A + f_E \phi_E \quad (3)$$

and

$$1 = f_A + f_E \quad (4)$$

Hence, ϕ_T , ϕ_A , and ϕ_E are the phase shifts observed for the mixture, pure Acryloid, and "pure" ester, respectively; f_A and f_E are the unknown fractions of Acryloid and ester. These equations apply and were solved for each frequency. The equations can be combined to yield

$$f_E = \frac{\phi_T - \phi_A}{\phi_E - \phi_A} \quad (5)$$

and

$$f_A = \frac{\phi_T - \phi_E}{\phi_A - \phi_E} \quad (6)$$

The sample calculations for the ester-Acryloid mixture are given in Table I, showing a quite reasonable analysis. The data agree well enough to show that the method works, yet point out the need for more accurate phase measurements. This analysis and the numerical method are examined in more detail in Section IV.

TABLE I. ANALYSIS OF MIXTURE RESPONSE CURVES

f (Hz)	ϕ_T (deg)	ϕ_E (deg)	ϕ_A (deg)	f_A (%)	f_E (%)
930	120	152.5	95	43.5	56.5
1150	130	170	100	42.8	57.2
1650	150	175	120	54.5	45.5
2200	162.5	180	150	41.6	58.4

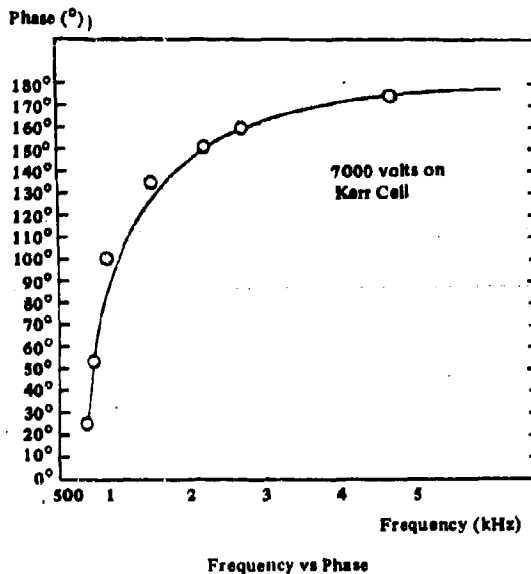


FIGURE 7. ESTER S-9 KERR RESPONSE CURVE

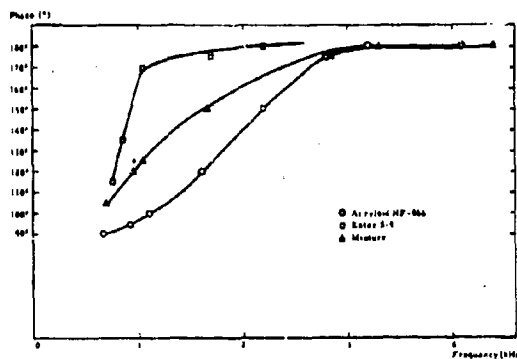


FIGURE 8. MIXTURE KERR RESPONSE CURVES (Un-Normalized)

SECTION IV

THEORETICAL MIXTURE ANALYSIS

A digital computer program for the solution of the general equations derived in Appendix IV has been written and used to calculate the Kerr response curves for multicomponent systems. The program requires as input data the number of constituents, their contribution to the D. C. Kerr constant, their relaxation times, and a defined frequency range. The Fortran IV version of this program is given in Appendix V. The results that have been obtained thus far are shown in Figures 9 through 21. In these figures, the curve labeled "Amplitude" is $B(\omega)$, that labeled "Derivative" is $dI(\omega)/d\omega$, that labeled "Phase" is $\delta(\omega)$, and "Intensity" is $I(\omega)$. The maximum magnitude that these variables have in any figure is given in parentheses after the label. This number thus defines the scale factor. The experimental observables are $I(\omega)$, $dI(\omega)/d\omega$, and $\delta(\omega)$. See Appendix VII for the equations for these quantities and their derivations. For convenience, Table II shows the input data for Figures 9 through 21.

The first three cases are single-component systems, included for the purpose of testing the simple additivity rules. The next three cases are two-component systems under moderate frequency resolution, and the last four are three-component systems under poor resolution conditions. The last case is a synthesis of the Acryloid HF-866 - Ester S-9 mixture experimental curves, based on measured relaxation times in the separated systems.

TABLE II. SUMMARY OF PARAMETERS USED
TO GENERATE FIGURES 9 THROUGH 21

Figure	Constituents	D.C. Kerr Effect Contribution	Relaxation Times (sec)	Frequency Range (radians/sec)
9	1	1.0	0.001	0-13000
10	1	1.0	0.0003	0-13000
11	1	1.0	0.0001	0-13000
12	2	0.5 0.5	0.001 0.0001	0-13000 0-13000
13	2	0.2 0.8	0.001 0.0001	0-13000
14	2	0.8 0.2	0.001 0.0001	0-13000
15	3	0.333 0.333 0.333	0.001 0.0003 0.0001	0-13000
16	3	0.2 0.2 0.6	0.001 0.0003 0.0001	0-13000
17	3	0.6 0.2 0.2	0.001 0.0003 0.0001	0-13000
18	3	0.2 0.6 0.2	0.001 0.0003 0.0001	0-13000
19	1	1.0	0.00055	0-9000
20	1	1.0	0.00093	0-9000
21	2	0.5 0.5	0.00055 0.00093	0-9000

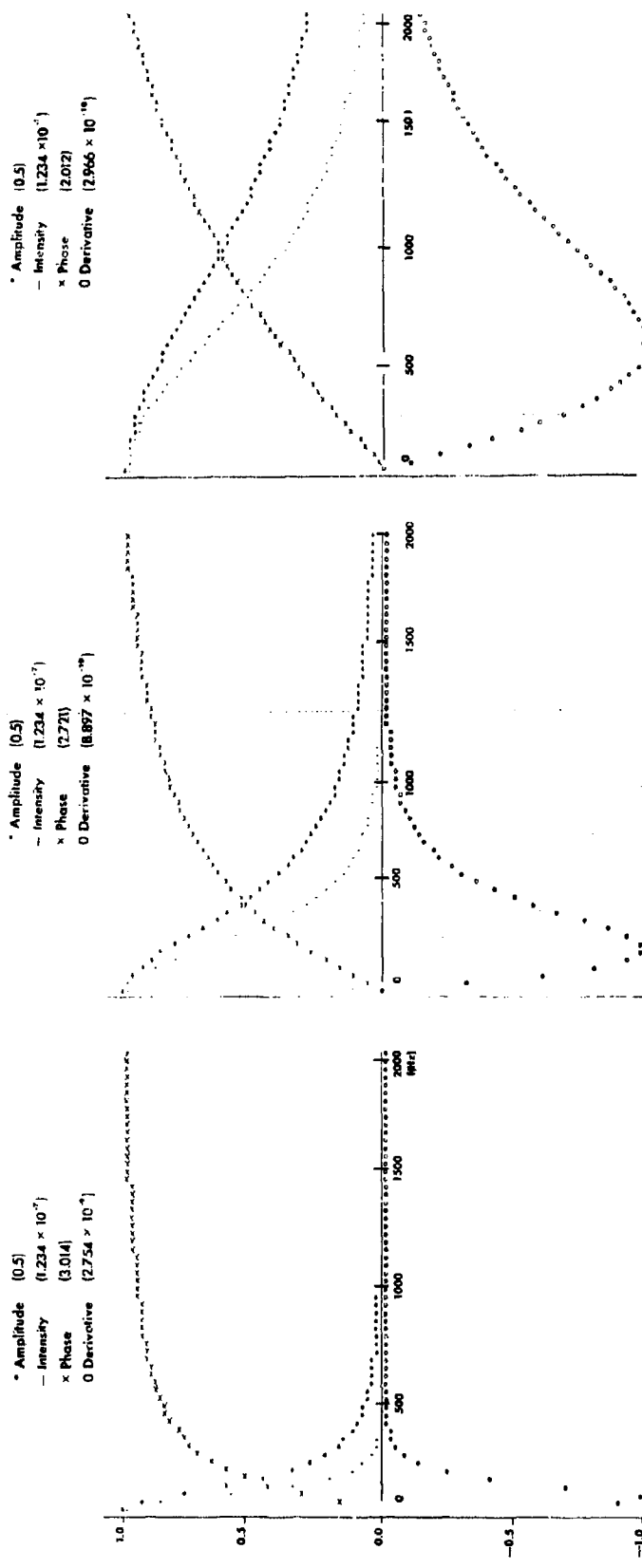


FIGURE 9. ONE-COMPONENT KERR RESPONSE CURVE

$\tau = 0.001$
 $C = 1.0$

All curves shown in Figures 9 through 21 are normalized.
 The maximum value of each variable is given in parentheses in the legend.

FIGURE 10. ONE-COMPONENT KERR RESPONSE CURVE

$\tau = 0.0003$
 $C = 1.0$

FIGURE 11. ONE-COMPONENT KERR RESPONSE CURVE

$\tau = 0.0001$
 $C = 1.0$

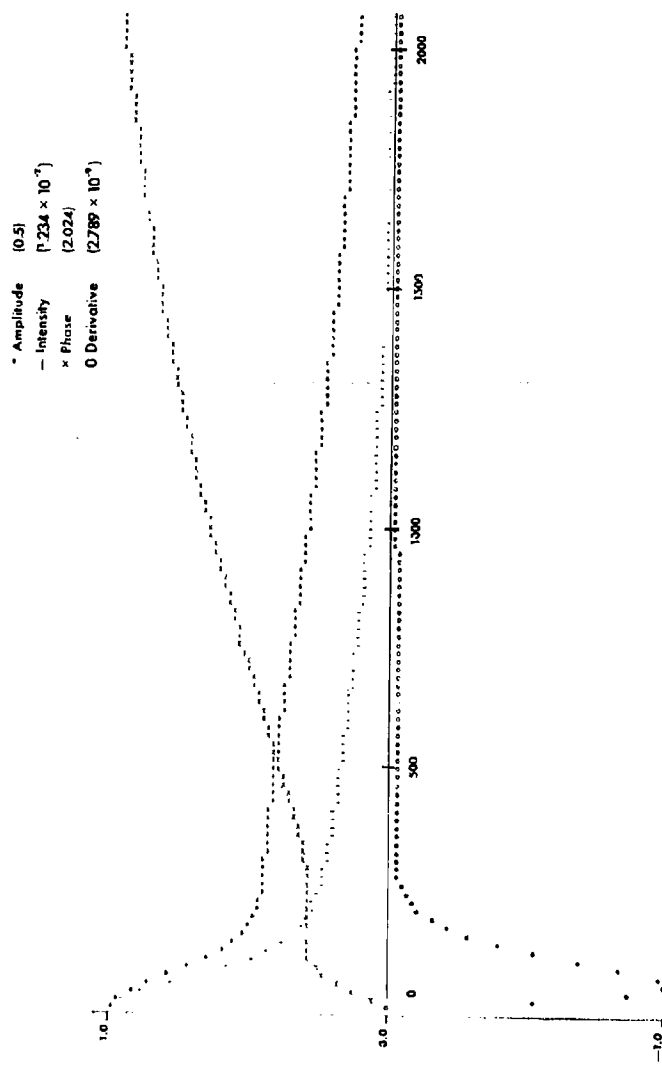


FIGURE 12. TWO-COMPONENT KERR RESPONSE CURVES

$\tau(1) = 0.001$ $\tau(2) = 0.0001$
 $C(1) = 0.5$ $C(2) = 0.5$

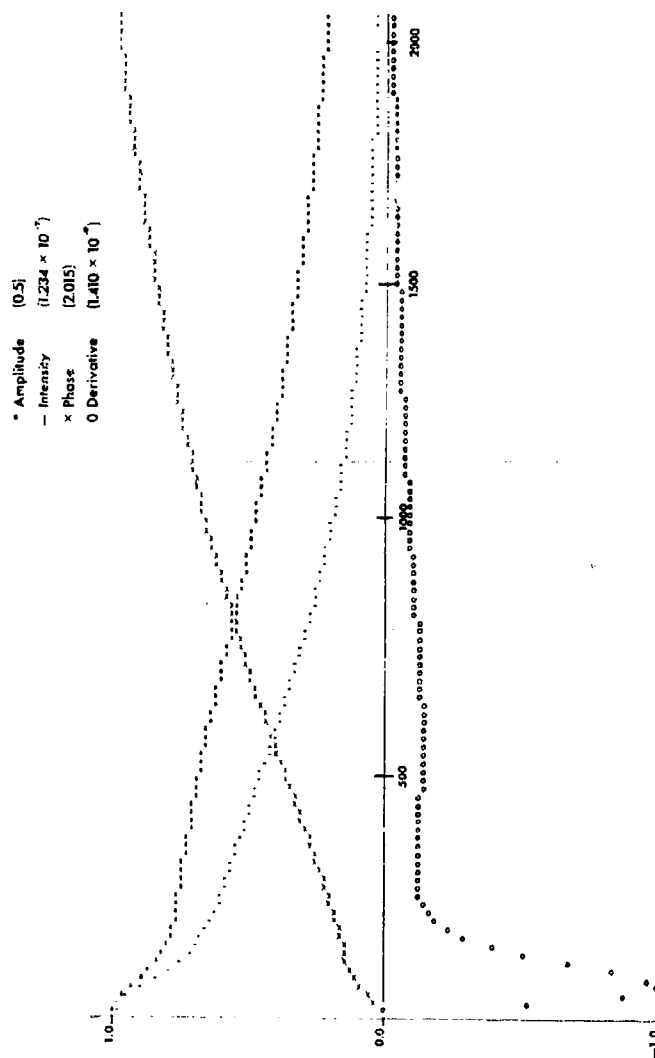


FIGURE 13. TWO-COMPONENT KERR RESPONSE CURVES

$$\begin{array}{ll}
 \tau_{(1)} = 0.001 & \tau_{(2)} = 0.0001 \\
 C_{(1)} = 0.2 & C_{(2)} = 0.8
 \end{array}$$

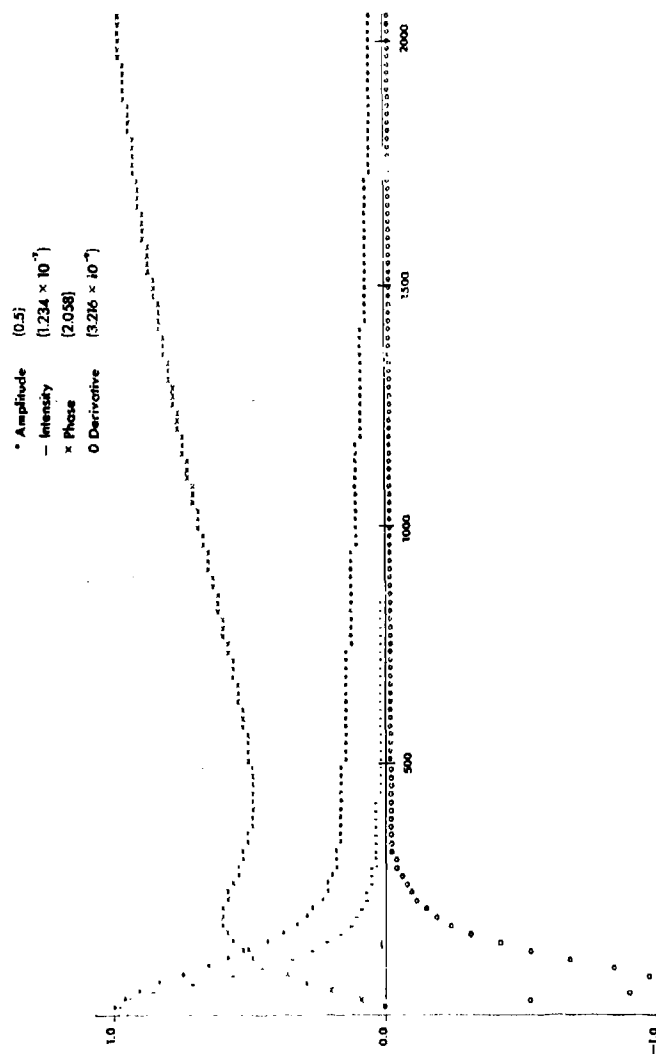


FIGURE 14. TWO-COMPONENT KERR RESPONSE CURVES

$$\begin{array}{ll}
 \tau_{(1)} = 0.001 & \tau_{(2)} = 0.0001 \\
 C_{(1)} = 0.8 & C_{(2)} = 0.2
 \end{array}$$

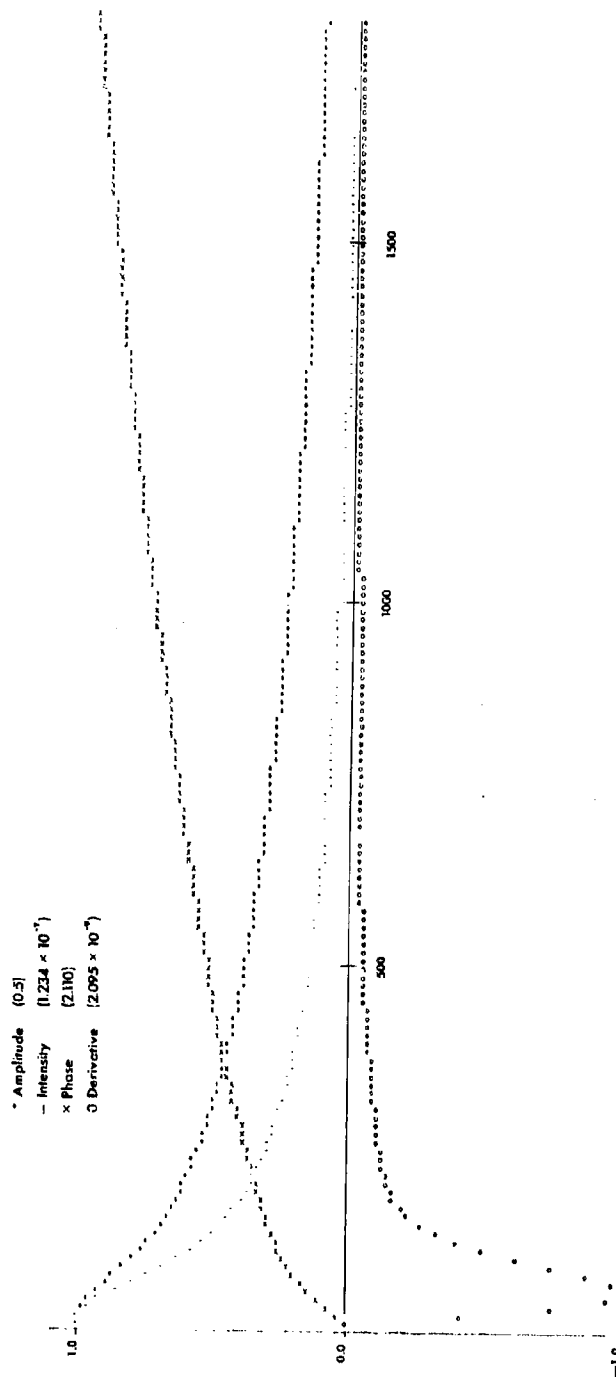


FIGURE 15. THREE-COMPONENT KERR RESPONSE CURVES

$$\begin{array}{ll}
 \tau(1) = 0.001 & \tau(2) = 0.0003 \\
 C(1) = 0.333 & C(2) = 0.333 \\
 & C(3) = 0.333
 \end{array}$$

* Amplitude (0.5)
 - Intensity (1.234×10^{-7})
 x Phase (2.047)
 o Derivative (1.469×10^{-6})

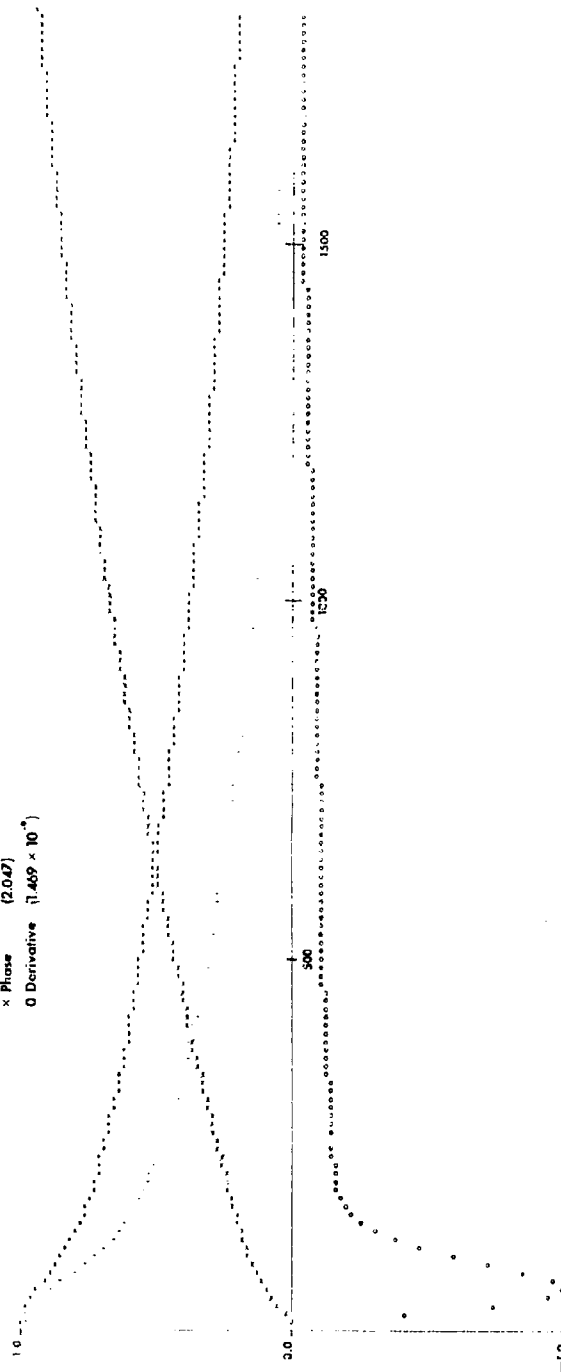


FIGURE 16. THREE-COMPONENT KERR RESPONSE CURVES

$\tau(1) = 0.001$ $\tau(2) = 0.0003$ $\tau(3) = 0.0001$
 $C(1) = 0.2$ $C(2) = 0.2$ $C(3) = 0.6$

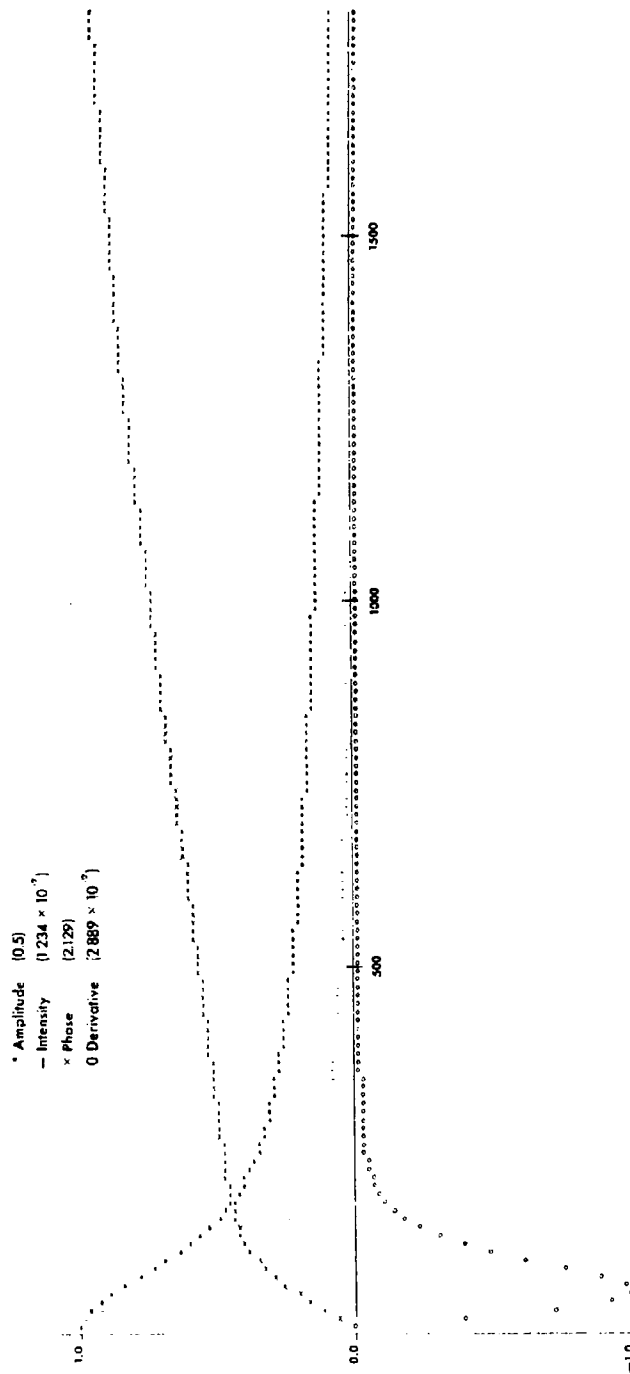


FIGURE 17. THREE-COMPONENT KERR RESPONSE CURVES

$\tau(1) = 0.001$ $\tau(2) = 0.0003$ $\tau(3) = 0.0001$
 $C(1) = 0.6$ $C(2) = 0.2$ $C(3) = 0.2$

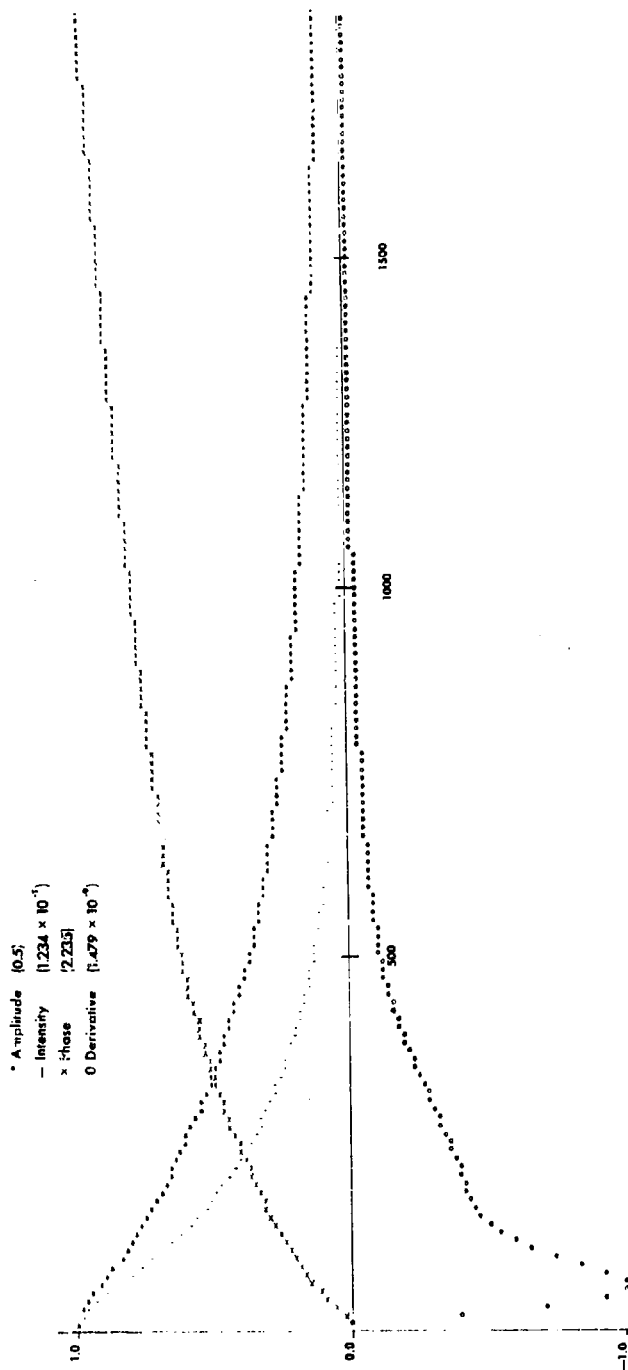


FIGURE 18. THREE-COMPONENT KERR RESPONSE CURVES

$$\begin{array}{ll}
 \tau(1) = 0.001 & \tau(2) = 0.0003 \\
 C(1) = 0.2 & C(2) = 0.6 \\
 & C(3) = 0.2
 \end{array}$$

Amplitude (0.5)
 Intensity (1.234×10^{-7})
 Phase (2.974)
 Derivative (1.631×10^{-6})

Amplitude (0.5)
 Intensity (1.234×10^{-7})
 Phase (3.042)
 Derivative (2.707×10^{-6})

Amplitude (0.5)
 Intensity (1.234×10^{-7})
 Phase (2.991)
 Derivative (2.268×10^{-6})

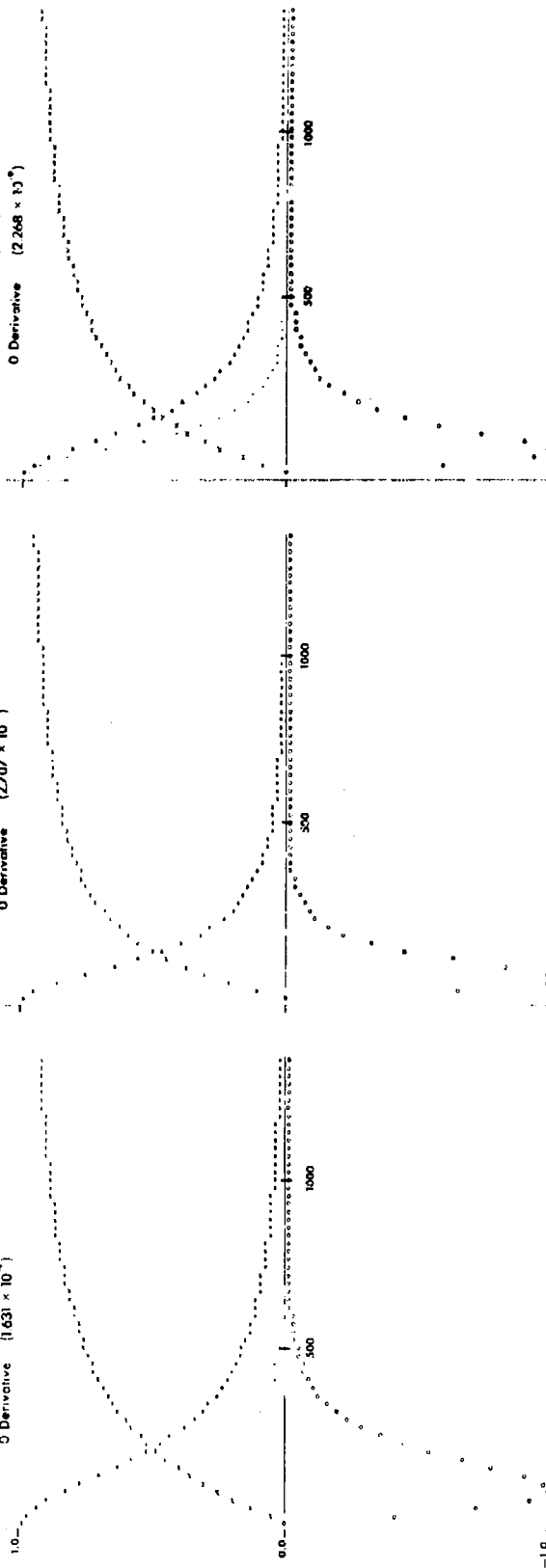


FIGURE 19. ONE-COMPONENT KERR RESPONSE CURVE

$\tau = 0.00055$
 $C = 1.0$

FIGURE 20. ONE-COMPONENT KERR RESPONSE CURVE

$\tau = 0.00093$
 $C = 1.0$

FIGURE 21. TWO-COMPONENT KERR RESPONSE CURVE

$\tau(1) = 0.00055$
 $C(1) = 0.5$
 $\tau(2) = 0.00093$
 $C(2) = 0.5$

These curves have been generated to find (1) the value of the differential spectrometer, (2) the methods of obtaining the concentration data, and (3) the concentration and frequency resolution possible under different conditions. From a study of the two-component curves, it can be seen that the differential method offers a real advantage when the low frequency component is the low concentration one (Figure 13). However, in the opposite case (Figure 14), the phase measurement seems to be the best analytical method. Basically, this reversal of character occurs because the dispersion region widens as frequency increases, thus lowering $dt/d\omega$. Therefore, as it is now conceived, the derivative method appears most useful when the lower concentration component is in the low frequency region.

In general, the concentration data should be obtained by analyzing the experimental data in terms of the equations of Appendix IV. Various methods of using nonlinear least squares fits and varying the test parameters have been used in this type of analysis. One in particular, Levenberg's method, has been used by the author to obtain the best fit and statistical data from electron spin resonance saturation curves with excellent results. However, it would be more appropriate to be able to obtain at least approximate concentration data from the curves themselves without resorting to computer analysis. To this end, the errors involved in the phase additivity and amplitude additivity methods have been estimated. The numbers from the single-component systems of appropriate relaxation times were multiplied by the concentrations used in the complete synthesis curve, added, and compared with the complete curve. The phase additivity method is governed by the equation

$$\phi_T(\omega) = \sum_i f_i \phi_i(\omega)$$

where f_i is the fraction of the i^{th} component in the system, ϕ_i is the phase shift of that component by itself, and ϕ_T is the total phase shift of the mixture. Similarly, the amplitude additivity method is defined by the equation

$$B_T(\omega) = \sum_i f_i B_i(\omega)$$

where $B_i(\omega)$ is the magnitude of the Kerr constant of the i^{th} component at any particular frequency, f_i is the fraction of the i^{th} component in the system, and $B_T(\omega)$ is the total Kerr constant.

TABLE III. SIMPLE ADDITIVITY RULES FOR MODERATE FREQUENCY RESOLUTION

$\tau_{(1)} = 0.001 \text{ sec}$ $\tau_{(2)} = 0.0001 \text{ sec}$

Frequency	0.8 X Phase (1)	0.2 X Phase (2)	Sum	Exact	0.8 X Amp (1)	0.2 X Amp (2)	Sum	Exact
0	0	0	0	0	0.4	0.1	0.5	0.5
34	0.422	0.011	0.433	0.429	0.37	0.1	0.47	0.46
69	0.788	0.022	0.810	0.781	0.306	0.1	0.41	0.38
103	1.08	0.032	1.11	1.03	0.24	0.099	0.34	0.29
172	1.475	0.054	1.529	1.24	0.14	0.098	0.24	0.17
241	1.72	0.075	1.79	1.21	0.008	0.096	0.18	0.12
310	1.87	0.095	1.96	1.11	0.059	0.094	0.15	0.10
379	1.98	0.115	2.09	1.04	0.042	0.091	0.13	0.088
448	2.06	0.135	2.19	1.03	0.0304	0.088	0.12	0.084
517	2.11	0.155	2.26	1.05	0.0236	0.085	0.11	0.082
586	2.16	0.17	2.33	1.09	0.0186	0.082	0.10	0.079
655	2.20	0.188	2.39	1.14	0.0151	0.078	0.093	0.077
723	2.25	0.22	2.47	1.25	0.0124	0.075	0.087	0.074
791	2.29	0.25	2.54	1.37	0.0075	0.064	0.071	0.065
1069	2.31	0.276	2.59	1.48	0.0058	0.058	0.063	0.059
1207	2.34	0.30	2.64	1.58	0.0045	0.052	0.056	0.053
1345	2.36	0.32	2.68	1.68	0.0037	0.047	0.051	0.048
1483	2.37	0.34	2.71	1.77	0.0030	0.042	0.045	0.043
1621	2.38	0.357	2.74	1.84	0.0026	0.038	0.040	0.039
1759	2.39	0.37	2.76	1.91	0.0022	0.034	0.036	0.036
1897	2.40	0.38	2.78	1.98	0.0019	0.031	0.033	0.032
2034	2.41	0.40	2.81	2.04	0.0016	0.038	0.030	0.029

Table III shows that, under moderate resolution ($\tau_1 = 10\tau_2$), a two-component system is not described by the phase additivity rule except at small angles (i.e., both δ_1 and $\delta_2 < 30$ degrees), but is adequately described by the amplitude additivity rules at both low and high frequencies. In the intermediate range, the canceling phase shift of the low frequency component causes the exact answer to be significantly less than the simple sum. However, at low frequencies, both signals are approximately in phase and hence add algebraically. Also, at high frequencies, the low frequency ($\tau = 0.001$ sec) component's amplitude is near zero, so that the only remaining amplitude contribution is from the high frequency ($\tau = 0.0001$ sec) component. This state of affairs is expected to be true for many component systems in which no relaxation time is nearer than a factor of ten to the others. Thus, under these resolution conditions, the simple amplitude additivity rules are expected to hold when the data are taken in low dispersion regions.

The data in Table IV show that the phase additivity rule is valid at least for two-component systems in which the relaxation times differ by less than a factor of two ($\tau_1 = 0.00055$ sec, $\tau_2 = 0.00093$ sec). The error at any frequency was 5 percent or less, even in regions of high dispersion. The data in Table IV also show that the amplitude additivity rules are approximately obeyed throughout the dispersion region. Thus, either simple method may be used with the noted reliability when the resolution is poor.

The limiting factors affecting the concentration analysis are (1) accuracy of the experimental data, (2) frequency resolution of the component critical frequencies, and (3) the basis of the analysis. In this section, the inaccuracy in the experimental data has been neglected completely. Also, the limits in obtaining concentration data under the various resolution conditions have not been fully explored.

TABLE IV. SIMPLE ADDITIVITY RULES FOR POOR FREQUENCY RESOLUTION

$\tau(1) = 0.0055$ sec $\tau(2) = 0.00093$ sec

Frequency	0.5 X Phase (1)	0.5 X Phase (2)	Sum	Exact	% Error (max)
0	0	0	0	0	—
48	0.203	0.334	0.537	0.532	1
95	0.389	0.603	0.992	0.966	2.5
143	0.549	0.798	1.347	1.296	4
191	0.682	0.936	1.618	1.548	5
239	0.790	1.037	1.827	1.748	5
286	0.879	1.117	1.991	1.908	5
334	0.952	1.169	2.121	2.038	5
382	1.013	1.215	2.228	2.146	4
430	1.064	1.252	2.316	2.236	4
477	1.106	1.281	2.387	2.313	4
525	1.143	1.306	2.449	2.378	3.5
573	1.174	1.328	2.502	2.434	3
621	1.202	1.346	2.548	2.483	2.5
668	1.226	1.361	2.587	2.526	2.5
716	1.247	1.374	2.621	2.564	2.5
Frequency	0.5 X Amp (1)	0.5 X Amp (2)	Sum	Exact	% Error (max)
0	0.250	0.250	0.500	0.500	—
48	0.239	0.222	0.461	0.458	1
95	0.212	0.167	0.379	0.372	2.5
143	0.179	0.119	0.298	0.290	3
191	0.148	0.0856	0.234	0.227	3.5
239	0.121	0.0628	0.184	0.179	3
286	0.0992	0.0474	0.147	0.143	3
334	0.0818	0.0368	0.119	0.116	3
382	0.0680	0.0292	0.0972	0.0956	2
430	0.0571	0.0237	0.080	0.0797	1.5
477	0.0485	0.0196	0.0681	0.0673	1.5
525	0.0416	0.0164	0.0580	0.0574	1.5
573	0.0359	0.0139	0.0498	0.0495	1
621	0.0313	0.0120	0.0433	0.0430	1
668	0.0275	0.0104	0.0379	0.0377	1
716	0.0243	0.0091	0.0334	0.0333	1

SECTION V

SUMMARY

It has been shown experimentally that the time lag or phase shift in the Kerr signal can be used to characterize certain molecules and also to analyze a particular two-component mixture of compounds. It has also been shown by numerical solution of the Kerr response curve for mixtures that the simple phase additivity rule breaks down when the relaxation times differ by a factor of 10, but hold for times differing by less than a factor of 2. The amplitude additivity holds in both cases if applied at the proper frequencies. Also, the calculated intensities and derivative spectra that were obtained under different concentration and frequency resolution conditions are presented for qualitative evaluation.

The primary requirement for the applicability of the method is that the compounds under study have either a permanent dipole moment or an anisotropic polarizability tensor. If either of these conditions is satisfied, the compound can be oriented by the electric field. In general, any compound that consists of different atoms which are not arranged symmetrically will have a permanent dipole moment. Also, any compound with less than cubic symmetry will have an anisotropic polarizability. Thus, in principle, the method is very general: the only exceptions being very symmetrical compounds like methane.

In practice, the method is limited by the high frequencies required to measure the critical frequencies of low molecular weight compounds and by the attainable electric fields. The present work has not reached the limit on either frequency or electric field. In order to facilitate the extension to higher frequency, a spectrometer has been designed which eliminates the need for high frequency detection electronic equipment. This spectrometer (shown in Appendix VI) uses a modulation technique to allow phase detection at a constant audio frequency while scanning the driving frequency through the range of the power amplifier. This scheme has the advantage of considerably reducing the difficulties involved in high frequency measurements. Preliminary tests of this concept are under way.

In the future, a temperature variation capability should be built into the apparatus. This would allow study of the geometry changes in the Acryloid HF-866 and other viscosity stabilizers as a function of temperature. Because temperature enters into the expression for the rotational diffusion constant, this capability would also allow manipulation of the critical frequencies. A compound that is outside the frequency range of the instrument could be brought in by lowering the sample temperature.

Experimentally, the resonance method which has been used in this work can be extended to much higher frequencies. The general requirement is that power oscillators be available at the frequency range required. The amount of power available from the oscillator, the frequency, and the quality of the components used then determines the electric field strengths involved and hence the Kerr signal amplitude. The only major difficulty in extending the frequency range of the current apparatus is the lack of high frequency phase lock in amplifier equipment.

Finally, our conclusions are that the different Kerr response curves of different molecules can in principle be used to analyze a chemical mixture. Aside from sensitivity considerations, the most important factors in any particular mixture are the relative relaxation times of the components and their relative zero frequency Kerr constants.

For instance, a compound such as the poly- γ -benzyl-L-glutamate can be measured at low frequencies but will not interfere with high frequency measurements of other species. The practical rule of thumb for observing obvious breaks in the Kerr response curve appears to be that the relaxation times differ by at least a factor of 10. Cases in which the ratio of relaxation times is less than 10 require numerical analysis of the mixture response curve by using control curves from the independent components. Obviously, such a procedure assumes that the components do not alter each other's response curves and hence the absence of any appreciable molecular interaction between components.

APPENDIX I

SIGNAL SHAPE ANALYSIS

The optical phase difference between components of the polarization vector parallel to and perpendicular to the electric field is given by

$$\delta = 2\pi j \ell F^2 \quad (1)$$

where j is the Kerr constant, ℓ the path length, and F the electric field strength. The amount of light passed by the analyzer is given by

$$I = I_o \sin^2 (\delta/2) \quad (2)$$

when the polarizer and analyzer are crossed.

Substituting (1) into (2), the result is

$$I = I_o \sin^2 (\pi j \ell F^2) \quad (3)$$

Using a trigonometric identity, the intensity is

$$I = \frac{I_o}{2} [1 - \cos(2\pi j \ell F^2)] \quad (4)$$

If

$$F = F_o \sin \omega t \quad (5)$$

$$\pi j \ell F_o^2 = k$$

then

$$I = \frac{I_o}{2} [1 - \cos(2k \sin^2 \omega t)] \quad (6)$$

Expanding $\sin^2 \omega t$, then

$$I = \frac{I_o}{2} \left[1 - \cos \left(\frac{2k}{2} (1 - \cos 2\omega t) \right) \right] \quad (7)$$

Expanding (7), the intensity becomes

$$I = \frac{I_o}{2} [1 - \cos k \cos(k \cos 2\omega t) - \sin k \sin(k \cos 2\omega t)] \quad (8)$$

Using

$$\left. \begin{aligned} \cos(r \cos \theta) &= J_0(r) + 2 \sum_{\substack{n \text{ even,} \\ \text{positive}}} I^n J_n(r) \cos(n\theta) \\ \sin(r \sin \theta) &= 2 \sum_{\substack{n \text{ odd,} \\ \text{positive}}} J_n(r) \sin(n\theta) \end{aligned} \right\} \quad (9)$$

where $J_n(r)$ is the cylindrical Bessel function, the total intensity becomes

$$I = \frac{I_0}{2} \left[1 - \cos k [J_0(k) + 2 \sum_{\substack{n \text{ even,} \\ \text{positive}}} i^n J_n(k) \cos(n2\omega t)] - \sin k [2 \sum_{\substack{n \text{ odd,} \\ \text{positive}}} i^{n+1} J_n(k) \cos(n2\omega t)] \right] \quad (10)$$

However, if the quantity measured is the component of I at frequency 2ω , the only surviving term is

$$I_{2\omega} = I_0 \sin(k) J_1(k) \cos 2\omega t \quad (11)$$

Using (5) to expand k , the result is

$$I_{2\omega} = I_0 \sin(\pi/2 F_0^2) J_1(\pi/2 F_0^2) \cos 2\omega t \quad (12)$$

Table V lists values of δ , $\sin \delta$, $J_1(\delta)$, and $\sin(\delta) \times J_1(\delta)$ for the range of interest. The magnitude of $I_{2\omega}$ is proportional to the product $\sin(\delta) \times J_1(\delta)$, so that the last column in Table II gives the normalized amplitude ($I_{2\omega}/I_0$) of the component at frequency 2ω . The maximum in this amplitude occurs at 1.7 radians, somewhat greater than the 90-degree point at 1.57 radians. The amplitude increases rapidly up to about 1.2 radians and any increase in δ over 1.2 is of questionable value.

It should be pointed out that this analysis assumes a particular Kerr constant at any given frequency. That is, the analysis here is strictly to show the dependence of the amplitude of the 2ω signal on the various experimental parameters at any particular frequency. For the frequency dependence of the Kerr constant and phase shift, refer to Benoit's paper in Appendix VII.

TABLE V. MODULATION PARAMETERS

δ (radians)	$\sin \delta$	$J_1(\delta)$	$\sin \delta \times J_1(\delta)$
0.0	0.0	0.0000	0.000
0.1	0.0998	0.0499	0.0050
0.2	0.1987	0.0995	0.0198
0.3	0.2955	0.1483	0.0438
0.4	0.3894	0.1960	0.0763
0.5	0.4794	0.2433	0.1166
0.6	0.5646	0.2867	0.1619
0.7	0.6442	0.3290	0.2119
0.8	0.7174	0.3688	0.2646
0.9	0.7833	0.4059	0.3179
1.0	0.8415	0.4401	0.3703
1.1	0.8912	0.4709	0.4197
1.2	0.9320	0.4983	0.4644
1.3	0.9636	0.5220	0.5030
1.4	0.9854	0.5419	0.5340
1.5	0.9927	0.5579	0.5538
1.57	1.0000	0.5663	0.5663
1.6	0.9996	0.5699	0.5697
1.7	0.9917	0.5778	0.5730
1.8	0.9738	0.5815	0.5663
1.9	0.9463	0.5812	0.5500
2.0	0.9093	0.5767	0.5244

APPENDIX II

THEORETICAL BASIS OF TIME LAGS

The theory for the dependence of the Kerr constant on the frequency of the applied electric field has been summarized by H. Benoit. Using the laws of Brownian motion and changing parameters according to the mechanism, he arrives at different results for the two orientation mechanisms. The orientation by a permanent moment leads to the result

$$\Delta n = \Delta n_0 \left[\frac{1}{1 + 9\omega^2 \tau^2 / 4} + \frac{\cos(2\omega t - \delta_2)}{\sqrt{1 + \omega^2 \tau^2} \sqrt{1 + 9\omega^2 \tau^2 / 4}} \right] \quad (1)$$

where Δn is the observed difference in indices of refraction, Δn_0 for d.c. voltages, $\tau = 1/(3D)$, D being the rotational diffusion constant, and

$$\tan \delta_2 = \frac{5\omega\tau}{2 - 3\omega^2 \tau^2} \quad (2)$$

For the case of orientation by an induced moment, the corresponding equation is

$$\Delta n = \Delta n_0 \left[1 + \frac{\cos(2\omega t - \delta_1)}{\sqrt{1 + \omega^2 \tau^2}} \right] \quad (3)$$

with

$$\tan \delta_1 = \omega\tau \quad (4)$$

In the case of the permanent moment orientation, the magnitude of the Kerr constant goes to zero as the frequency of the electric field increases, with the phase lag of the observed signal going to 180 degrees in the limit. By contrast, the induced moment Kerr constant goes to half the d.c. value and the phase lag goes to 90 degrees at high frequencies. The critical frequency in the permanent moment case is determined by finding the point at which the signal is shifted by 90 degrees and solving the equation for $\tan \delta_2 = \infty$. This leads to the equation

$$D = \frac{\omega}{\sqrt{6}} \quad (5)$$

For the case of an induced moment, the point at which the signal is shifted by 45 degrees is given by

$$D = \frac{\omega}{3} \quad (6)$$

the rotational diffusion time is given by Boeckel, et al.,* as

$$D \approx \frac{kT}{\eta L^3} (\log L - \log 0.8 R) \quad (7)$$

where L is the length of the molecule, R is the cross section dimension, and η is the viscosity of the solvent.

*Boeckel, G., Genzling, J., Weill, G., and Benoit, H., *J. Chim Phys*, **59**, 1962, 999.

APPENDIX III

EXPERIMENTAL CONSIDERATIONS

Figure 22 shows the electrical analogy of the Kerr system. The capacitor K in Figure 22 represents the Kerr cell; its capacitance is approximately 100 pf. This capacitance K may be neglected in the linear analysis, since it is in parallel with a much larger capacitor and thus contributes little to the total capacitance of the circuit. In other words, K acts as an open circuit at low frequencies.

The inductor L_1 (decoupling transformer) in Figure 22 acts as a short circuit below 3 kHz and the capacitor C_2 is chosen to act as a short above 3 kHz so that these two components have little effect on the operation of the circuit shown in Figure 22.

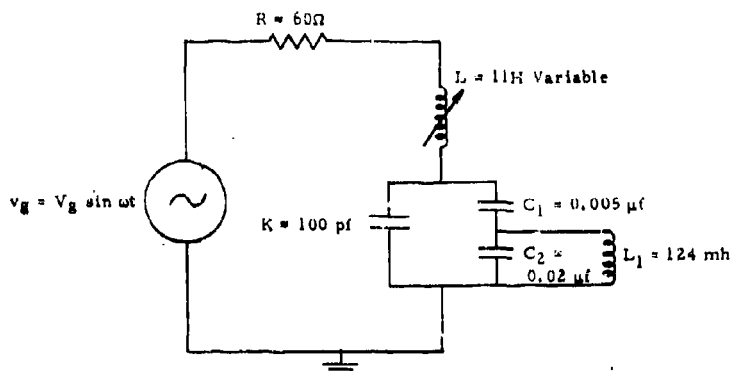


FIGURE 22. ELECTRICAL ANALOGY OF THE KERR SYSTEM

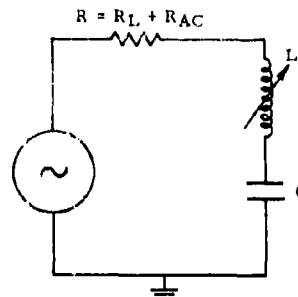


FIGURE 23. A SIMPLE R-L-C CIRCUIT

The electrical circuit under these assumptions can be represented as a simple R-L-C circuit as shown in Figure 23.

In Figure 23, R represents the real and a.c. resistance basically in the inductor L . The total resistance R is approximately 60 ohms at low frequencies. The simple R-L-C circuit in Figure 23 can be tuned for resonance by varying the inductor L which is an 11-henry variable inductor. In the R-L-C circuit of Figure 23, use is made of series resonance to produce the large driving voltages that are necessary for laser intensity modulation in the Kerr cell.

The loop equation for the circuit in Figure 23, assuming zero initial conditions, is

$$L \frac{di}{dt} + Ri + \frac{1}{C} \int_0^t i \, dt = v_g \quad (1)$$

The complementary function, or the transient part of the current in Equation (1), is independent of the excitation and can be found from the homogeneous equation in operator notation:

$$LD^2 + RD + \frac{1}{C} i_{tr} = 0 \quad (2)$$

The characteristic equation corresponding to Equation (2) is

$$Ls^2 + Rs + \frac{1}{C} = 0 \quad (3)$$

which has two roots:

$$s_1 = -\frac{R}{2L} + \sqrt{\left(\frac{R}{2L}\right)^2 - \frac{1}{LC}} = -\alpha + b$$

$$s_2 = -\frac{R}{2L} - \sqrt{\left(\frac{R}{2L}\right)^2 - \frac{1}{LC}} = -\alpha - b$$

Therefore

$$i_{tr} = K_1 e^{s_1 t} + K_2 e^{s_2 t} \quad (4)$$

where K_1 and K_2 are two arbitrary constants to be determined from two initial conditions when t is determined.

In solving for the transient condition, three different situations are possible depending on the values of R , L , and C .

(Case i)

$$\left(\frac{R}{2L}\right)^2 > \frac{1}{LC}, \text{ or } R > 2\sqrt{\frac{L}{C}}; \text{ } b \text{ is real}$$

$$i_{tr} = e^{-\alpha t}(K_1 e^{bt} + K_2 e^{-bt}) \quad (5)$$

Since $\alpha > b$, the transient current consists of two exponentially decreasing components with different rates of decay. This is called the overdamped case and occurs when the resistance in the circuit of Figure 23 is large. The exponential function of Equation (4) with real components can be expressed in terms of hyperbolic sines and cosines.

$$e^{bt} = \cosh bt + \sinh bt$$

$$e^{-bt} = \cosh bt - \sinh bt$$

i_{tr} is then

$$i_{tr} = e^{-\alpha t}(A_1 \cosh bt + A_2 \sinh bt) \quad (6)$$

where the constants A_1 and A_2 stand for $(K_1 + K_2)$ and $(K_1 - K_2)$, respectively.

(Case ii)

$$\left(\frac{R}{2L}\right)^2 = \frac{1}{LC}, \text{ } R = 2\sqrt{\frac{L}{C}}; \text{ } b = 0$$

Under this condition, the characteristic Equation (3) has a double root, and the transient solution becomes

$$i_{tr} = (K_1 + K_2)e^{-\alpha t} \quad (7)$$

The two terms in Equation (7) are non-oscillatory.

(Case iii)

$$\left(\frac{R}{2L}\right)^2 < \frac{1}{LC} : R < 2\sqrt{\frac{L}{C}} : b \text{ is imaginary}$$

$$b = j \sqrt{\frac{1}{LC} - \left(\frac{R}{2L}\right)^2} = j\beta$$

$$i_{tr} = e^{-\alpha t} (K_1 e^{j\beta t} + K_2 e^{-j\beta t}) \quad (8)$$

Now

$$e^{j\beta t} = \cos \beta t + j \sin \beta t \quad (9)$$

$$e^{-j\beta t} = \cos \beta t - j \sin \beta t \quad (10)$$

Substituting Equations (9) and (10) into Equation (8) gives

$$i_{tr} = e^{-\alpha t} (A_1 \cos \beta t + A_2 \sin \beta t) \quad (11)$$

Equation (11) is the case of the transient current in the Kerr resonant circuit in which $R < 2\sqrt{L/C}$ where C is approximately $10^{-9}F$ and L is a variable 11-henry inductor. This case is called the underdamped case and occurs when the resistance in the circuit is small.

The steady-state solution can be determined from Equation (1) when $v_g = V_g \sin \omega t$.

The impedance concept is simplest to use when an applied voltage is sinusoidal. The impedance of a series R-L-C circuit to a current of angular frequency ω is

$$Z = R + j\omega L + \frac{1}{j\omega C} = |Z| e^{j\theta_z} \quad (12)$$

where

$$|Z| = \sqrt{R^2 + \left(\omega L - \frac{1}{\omega C}\right)^2} \quad (13)$$

and

$$\theta_z = \tan^{-1} \frac{\omega L - \frac{1}{\omega C}}{R} \quad (14)$$

The steady-state current, then, is

$$i_{ss} = \frac{V_g}{|Z|} \sin(\omega t - \theta_z)$$

$$= \frac{V_g}{\sqrt{R^2 + \left(\omega L - \frac{1}{\omega C}\right)^2}} \sin\left(\omega t - \tan^{-1} \frac{\omega L - \frac{1}{\omega C}}{R}\right) \quad (15)$$

The total current i is the sum of i_{ss} in Equation (15) and i_{tr} in Equation (11):

$$i = i_{tr} + i_{ss} \quad (16)$$

$$i = e^{-\alpha t} (A_1 \cos \beta t + A_2 \sin \beta t) + \frac{V_g}{|Z|} \sin (\omega t - \theta_z) \quad (17)$$

To solve for the constants A_1 and A_2 , the initial conditions of the circuit in Figure 23 must be known. In the Kerr system, $i(0) = 0$ and $q(0) = 0$; therefore, from Equation (17) at $t = 0$,

$$\begin{aligned} 0 &= A_1 - \frac{V_g}{|Z|} \sin \theta_z \\ A_1 &= \frac{V_g}{|Z|} \sin \theta_z \end{aligned} \quad (18)$$

Knowing that $q = (di/dt)$, A_2 can be solved for by differentiating Equation (17) and letting (di/dt) equal zero since

$$q(0) = \frac{di}{dt}(0) = 0$$

or

$$L \frac{di}{dt} = -\frac{V_g}{L} \sin \omega t$$

and at $t = 0$

$$\frac{di}{dt} = \frac{V_g}{L} \sin 0 = 0 \quad (19)$$

Differentiating Equation (18) gives:

$$\begin{aligned} \frac{di}{dt} &= e^{-\alpha t} (-A_1 \beta \sin \beta t + \beta A_2 \cos \beta t) \\ &\quad - (A_1 \cos \beta t + A_2 \sin \beta t) \alpha e^{-\alpha t} \\ &\quad + \frac{V_g}{|Z|} \omega \cos (\omega t - \theta_z) \end{aligned} \quad (20)$$

Substituting Equation (19) into Equation (20) at $t = 0$ gives

$$0 = \beta A_2 - \alpha A_1 + \frac{V_g}{|Z|} \omega \cos \theta_z \quad (21)$$

Replacing A_1 with Equation (18) in Equation (21) gives

$$\begin{aligned} 0 &= \beta A_2 - \alpha \frac{V_g}{|Z|} \sin \theta_z + \frac{V_g}{|Z|} \omega \cos \theta_z \\ A_2 &= \frac{V_g}{\beta |Z|} (\alpha \sin \theta_z - \omega \cos \theta_z) \end{aligned} \quad (22)$$

Replacing A_1 and A_2 in Equation (17) with their equalities gives the complete equation for the total current in the circuit of Figure 23:

$$i = \frac{V_g}{|Z|} \left\{ e^{-\alpha t} \left[\sin \theta_z \cos \beta t + \frac{(\alpha \sin \theta_z - \omega \cos \theta_z)}{\beta} \sin \beta t \right] + \sin (\omega t - \theta_z) \right\} \quad (23)$$

By knowing the appropriate values of the components in the R-L-C circuit of Figure 23, one can determine the current and voltage as a function of time by using Equation (23). The transient current will become more important at high frequencies when the circuit in Figure 23 is pulsed with a high voltage spike.

The magnitude of the steady-state current in a series R-L-C circuit with respect to frequency is

$$|i_{ss}| = \frac{V_g}{\sqrt{R^2 + \left(\omega L - \frac{1}{\omega C} \right)^2}} \quad (24)$$

It can be seen that $|i_{ss}|$ is maximum at an angular frequency ω_R where

$$\omega_R L - \frac{1}{\omega_R C} = 0$$

or

$$\omega_R = \frac{1}{\sqrt{LC}} \quad (25)$$

In terms of frequency,

$$f_R = \frac{\omega_R}{2\pi} = \frac{1}{2\pi\sqrt{LC}} \quad (26)$$

In Equation (26), f_R is denoted as the resonant frequency. The maximum value of $|i_{ss}|$ can be denoted by I_m . Then, at resonance,

$$\left. \begin{aligned} |Z| &= R \\ \theta_z &= 0 \\ I_m &= \frac{V_g}{R} \end{aligned} \right\} \quad (27)$$

In Figure 24, typical curves for normalized current magnitude are plotted, $|i_{ss}|/I_m$ for two values of R . The magnitude of the steady-state current decreases as frequency of the applied voltage deviates from the resonant frequency, but the rate of decrease is slower for a circuit with a higher resistance.

The concept of continuous driving of an L-C tuned circuit has proven to be a useful one in the experimental work to date. Voltages in excess of the breakdown voltage of the inductors have been achieved from a 75-w oscillator. When extensions of the concept are considered, it becomes apparent that the situation does not deteriorate until frequencies of over 1 MHz are considered. For instance, at 1 MHz, a Q of approximately 100 can be obtained with relative ease. Also, an inductor of 3 mH will resonate with a 10-pF capacitor, leading to a resistance of 180 ohms. For a 10-w oscillator, the current will be 3000 v. Our cell separation is 3mm, giving 10,000 v/cm as the field strength across the cell. The pertinent equations are:

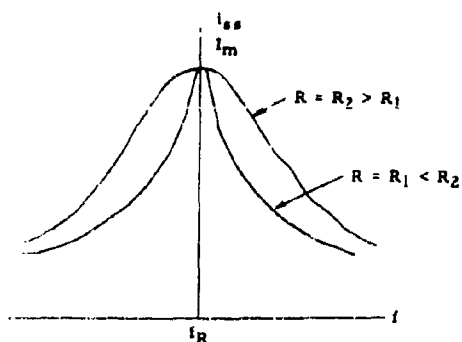


FIGURE 24. RESONANCE CURRENT CURVES FOR A SERIES R-L-C CIRCUIT

$$\left. \begin{aligned} Q &= \frac{\omega L}{R} \\ I &= \frac{1}{2\pi\sqrt{LC}} \\ V &= V_R + V_C + V_L \\ V &= I \left(R + j\omega L + \frac{1}{j\omega C} \right) \end{aligned} \right\} \quad (28)$$

At frequencies over 1 MHz, the power requirements for continuous driving become too stringent. At 10 MHz, a 10-w oscillator driving a 30- μ H, 10-pF tank circuit, would yield only 3600 v/cm. This difficulty may be alleviated by using a triggered thyatron to increase the peak power into the circuit. The thyatron would be triggered to put its power into the circuit in a very short time (less than 0.2 cycle), but would do this at a low frequency. If the thyatron delivered an average power of 10 w but did this in equal pulses (at 100 pulses/sec) which were 0.1 cycle wide at 10 MHz, the peak power into the circuit would be 10^7 w.

The peak power during the pulse may be cut down by increasing the repetition rate so that the power/pulse goes down. This can be done, if necessary, to avoid breakdown from very high peak voltages. The mathematical analysis of the signal waveform resulting from a pulsed system like this becomes very complicated.

APPENDIX IV

DERIVATION OF THE MIXTURE EQUATIONS

The basis of the analysis is that the separate components of the mixture do not interact significantly with each other. That is, each component is assumed to move independently of the others. This is a reasonable assumption for materials which do not form intermolecular hydrogen bonds, charge transfer complexes, etc.

Under this assumption, we may write*

$$\Delta n(\omega) = \sum_i c_i \Delta n_i(\omega) \quad (1)$$

where $\Delta n(\omega)$ is the total Kerr constant (written as the difference in indices of refraction), c_i is the concentration of the i th component, and $\Delta n_i(\omega)$ is the Kerr constant of the i th component.

At $\omega = 0$, Equation (1) becomes

$$\Delta n(0) = \sum_i c_i \Delta n_i(0) \quad (2)$$

where

$$\Delta n_i(\omega) = \Delta n_i(0) f_i(\omega) \quad (3)$$

Equation (3) is from Benoit's paper, with $f_i(\omega)$ being given for molecules with a permanent electric dipole moment as

$$f_i(\omega) = \frac{1}{2(1 + 9\omega^2 \tau_i^2/4)} + \frac{\cos(2\omega t - \delta_i)}{2\sqrt{1 + \omega^2 \tau_i^2} \sqrt{1 + 9\omega^2 \tau_i^2/4}} \quad (4)$$

$$\delta_i = \tan^{-1} \frac{5\omega \tau_i}{2 - 3\omega^2 \tau_i^2}$$

We can then form

$$\frac{\Delta n(\omega)}{\Delta n(0)} = \frac{\sum_i c_i \Delta n_i(0) f_i(\omega)}{\sum_i c_i \Delta n_i(0)} \quad (5)$$

which will give the normalized Kerr constant as a function of frequency. If we use the trigonometric identity $\cos(x - y) = \cos x \cos y + \sin x \sin y$ in Equation (4) and insert Equation (4) in Equation (5), we get

$$\frac{\Delta n(\omega)}{\Delta n(0)} = \left\{ \sum_i c_i \Delta n_i(0) \left[\frac{1}{2(1 + 9\omega^2 \tau_i^2/4)} + \frac{\cos \delta_i \cos 2\omega t}{2\sqrt{1 + \omega^2 \tau_i^2} \sqrt{1 + 9\omega^2 \tau_i^2/4}} \right. \right. \\ \left. \left. + \frac{\sin \delta_i \sin 2\omega t}{2\sqrt{1 + \omega^2 \tau_i^2} \sqrt{1 + 9\omega^2 \tau_i^2/4}} \right] \right\} / \sum_i c_i \Delta n_i(0) \quad (6)$$

If Equation (6) is put into the form:

*In terms of the Kerr constant of Appendix I, $f(\omega) = [\Delta n(\omega)/\lambda E^2]$.

$$\frac{\Delta n(\omega)}{\Delta n(0)} = A + B \cos(2\omega t - \delta) \quad (7)$$

then

$$A(\omega) = \left[\sum_i \frac{c_i \Delta n_i(0)}{2(1 + 9\omega^2 \tau_i^2/4)} \right] / \sum_i c_i \Delta n_i(0) \quad (8)$$

$$B(\omega) = \left\{ \left[\sum_i \frac{c_i \Delta n_i(0) \cos \delta_i}{2\sqrt{1 + \omega^2 \tau_i^2} \sqrt{1 + 9\omega^2 \tau_i^2/4}} \right]^2 + \left[\sum_i \frac{c_i \Delta n_i(0) \sin \delta_i}{2\sqrt{1 + \omega^2 \tau_i^2} \sqrt{1 + 9\omega^2 \tau_i^2/4}} \right]^2 \right\}^{1/2} / \sum_i c_i \Delta n_i(0) \quad (9)$$

and

$$\delta(\omega) = \tan^{-1} \left[\sum_i \frac{c_i \Delta n_i(0) \sin \delta_i}{2\sqrt{1 + \omega^2 \tau_i^2} \sqrt{1 + 9\omega^2 \tau_i^2/4}} \right] / \left[\sum_i \frac{c_i \Delta n_i(0) \cos \delta_i}{2\sqrt{1 + \omega^2 \tau_i^2} \sqrt{1 + 9\omega^2 \tau_i^2/4}} \right] \quad (10)$$

Beginning with the basic equation,

$$I = I_0 \sin^2 \delta/2 \quad (11)$$

and the relation for optical phase difference,

$$\delta = \frac{2\pi \ell}{\lambda} \Delta n \quad (12)$$

and substituting (7) into (12) and then (12) into (11), we have

$$I = I_0 \sin^2 \left[\frac{\pi \ell \Delta n(0)}{\lambda} A + \frac{\pi \ell \Delta n(0)}{\lambda} B \cos(2\omega t - \delta) \right] \quad (13)$$

To simplify notation, we let

$$A' = \frac{\pi \ell \Delta n(0)}{\lambda} A \quad \text{and} \quad B' = \frac{\pi \ell \Delta n(0)}{\lambda} B$$

Using $\sin^2 x = (1/2)(1 - \cos 2x)$ and then $\cos(x + y) = \cos x \cos y - \sin x \sin y$, we have

$$I = \frac{I_0}{2} \left\{ 1 - \cos(A') \cos[B' \cos(2\omega t - \delta)] + \sin(A') \sin[B' \cos(2\omega t - \delta)] \right\} \quad (14)$$

Using identity (9) in Appendix I, the relationship becomes

$$I = \frac{I_0}{2} \left\{ 1 - \cos(A') [J_0(B') + 2 \sum_{\substack{n \text{ even} \\ \text{positive}}} i^n J_n(B') \cos(n2\omega t - n\delta)] \right. \\ \left. + \sin(A') [2 \sum_{\substack{n \text{ odd} \\ \text{positive}}} i^{n+1} J_n(B') \cos(n2\omega t - n\delta)] \right\} \quad (15)$$

Selecting the 2ω component, the expression is

$$I_{2\omega} = I_0 \sin(A') J_1(B') \cos(2\omega t - \delta) \quad (16)$$

The derivative of Equation (16) is given by:

$$\frac{d|I_{2\omega}|}{d\omega} = \frac{I_0}{2} \left\{ \cos(A') J_1(B') \frac{dA'}{d\omega} + [\sin(A') J_0(B') - \sin A' J_1(B')/B'] \frac{dB'}{d\omega} \right\} \quad (17)$$

where

$$\begin{aligned} \frac{dA'}{d\omega} &= \frac{\frac{9\pi k \Delta n(0)}{4\lambda} \left[\frac{\sum_i c_i \Delta n_i(0) \omega \tau_i^2}{(1 + 9\omega^2 \tau_i^2/4)^2} \right]}{\sum_i c_i \Delta n_i(0)} \\ \frac{dB'}{d\omega} &= \frac{\pi^2 k^2 \Delta n^2(0)}{\lambda^2 B'} \left(f_1 \frac{df_1}{d\omega} + f_2 \frac{df_2}{d\omega} \right) / \left(\sum_i c_i \Delta n_i(0) \right)^2 \\ f_1 &= \sum_i \frac{c_i \Delta n_i(0) \cos \delta_i}{\sqrt{1 + \omega^2 \tau_i^2} \sqrt{1 + 9\omega^2 \tau_i^2/4}} \\ \frac{df_1}{d\omega} &= \sum_i \frac{c_i \Delta n_i(0)}{\sqrt{1 + \omega^2 \tau_i^2} \sqrt{1 + 9\omega^2 \tau_i^2/4}} \left\{ -\sin \delta_i(\omega) \frac{d\delta_i(\omega)}{d\omega} \right. \\ &\quad \left. - \cos \delta_i(\omega) \left[\frac{9\omega \tau_i^2}{4(1 + 9\omega^2 \tau_i^2/4)} + \frac{\omega \tau_i^2}{(1 + \omega^2 \tau_i^2)} \right] \right\} \\ f_2 &= \sum_i \frac{c_i \Delta n_i(0) \sin \delta_i}{\sqrt{1 + \omega^2 \tau_i^2} \sqrt{1 + 9\omega^2 \tau_i^2/4}} \\ \frac{df_2}{d\omega} &= \sum_i \frac{c_i \Delta n_i(0)}{\sqrt{1 + \omega^2 \tau_i^2} \sqrt{1 + 9\omega^2 \tau_i^2/4}} \left\{ \cos \delta_i(\omega) \frac{d\delta_i(\omega)}{d\omega} - \sin \delta_i(\omega) \right. \\ &\quad \left. \left[\frac{9\omega \tau_i^2}{4(1 + 9\omega^2 \tau_i^2/4)} + \frac{\omega \tau_i^2}{(1 + \omega^2 \tau_i^2)} \right] \right\} \end{aligned}$$

and

$$\frac{d\delta_i}{d\omega} = \frac{1}{\left(1 + \frac{5\omega \tau_i}{2 - 3\omega^2 \tau_i^2} \right)^2} \frac{10\tau_i + 15\omega^2 \tau_i^2}{(2 - 3\omega^2 \tau_i^2)^2} \quad (18)$$

APPENDIX V

COMPUTER PROGRAM FOR NUMERICAL EVALUATION OF MIXTURE EQUATIONS

```

PROGRAM MAIN(INPUT,OUTPUT,TAPE60=INPUT)
DIMENSION DBDW(600),PHASE(600),INTENS(600),FREQ(600),C(10),TAU(10)
DIMENSION AMP(600)
COMMON AMP,PHASE,INTENS,FREQ,C,TAU,DBDW
REAL INTENS
1001 CONTINUE
PRINT 99
99 FORMAT(1H1)
READ 100,N,(TAU(I),I=1,N)
PRINT 200,N,(TAU(I),I=1,N)
200 FORMAT(1X,22HNUMBER OF CONSTITUENTS,13,24HRELAXATION TIMES (SEC-1
9),10F7.5)
READ 101,(C(I),I=1,N)
PRINT 201,(C(I),I=1,N)
201 FORMAT(5X,14HCONCENTRATIONS,10F7.5)
100 FORMAT(2X,12,10F7.5)
READ 101,WMIN,WMAX
PRINT 111,WMIN,WMAX
111 FORMAT(5X,24HFREQUENCY RANGE IS FROM ,F7.0,2HTO,F7.0)
101 FORMAT(10F7.0)
RM=N
DEL = (WMAX-WMIN)/(60.*RM)
W = WMIN
I = 1
1 CALL EQUAT(I,N,W)
FREQ(I) = W/(2.*3.1416)
W = W+DEL
I = I+1
NN = I
IF (W .LE. WMAX) GO TO 1
NN = NN-1
C PRINT 102,(I,AMP(I),PHASE(I),INTENS(I),FREQ(I),I=1,NN)
C 102 FORMAT(2X,12,4E20.5)
CALL KERRPL(NN,0,1)
READ 101,CASPER
IF (EOF,60) 1000,1001
1000 CONTINUE
STOP
END
SUBROUTINE EQUAT(LL,N,W)
DIMENSION DBDW(600),PHASE(600),INTENS(600),FREQ(600),C(10),TAU(10)
DIMENSION AMP(600)
COMMON AMP,PHASE,INTENS,FREQ,C,TAU,DBDW
REAL INTENS
IF (LL .NE. 1) GO TO 1
SCORE = 0.
DO 2 I=1,N
2 SCORE = SCORE+C(I)
1 CONTINUE
A=0.
DADW=0.
ST = 0.
CT = 0.
CTP=0.
STP = 0.
DO 11 I = 1,N
X = 5.*W*TAU(I)/(2.-3.*W*W*TAU(I)*TAU(I))
DEL = ATAN(X)
IF (DEL .LT. 0.0) DEL = DEL+3.14159
Y = 1+W*W*TAU(I)*TAU(I)
Z = 1+9.*W*W*TAU(I)*TAU(I)/4.
DDELW=((10.*TAU(I) +15.*W*W*TAU(I)**3)/(2.-3.
9 *W*W*TAU(I)*TAU(I)**2 )/(1+X*X)
CTP=CTP+(C(I)/SQRT(Y*Z))*(-SIN(DEL)*DDELW-COS(DEL)*(9.*W

```

```

9 *TAU(I)*TAU(I)/(4.*Z)+W*TAU(I)*TAU(I)/Y))
STP=STP+(C(I)/SQRT(Y*Z))*(COS(DEL)*DDELW-SIN(DEL)*(9.*W*TAU(I)*
9 TAU(I)/(4.*Z)+W*TAU(I)*TAU(I)/Y))
DADW =DADW -C(I)*9.*W*(TAU(I)**2)/((2.*Z)**2)
A = A+C(I)/(2.*Z)
CT = CT+C(I)*COS(DEL)/(2.*SQRT(Y*Z))
11 ST = ST+C(I)*SIN(DEL)/(2.*SQRT(Y*Z))
A=A/SCORE
DADW=DADW/SCORE
C PRINT 100,LL,X,DEL,Y,Z,CT,ST,SCORE,W
R = SQRT(CT*CT+ST*ST)/SCORE
DBOW(LL)=(CT*CTP+ST*STP)/(SCORE*SCORE*B)
PHASE(LL) = ATAN(ST/CT)
IF (PHASE(LL) .LT. 0.) PHASE(LL)=PHASE(LL)+3.14159
A = 3.14159*.001*A
H = 3.14159*.001*H
AMP(LL)=B
INTENS(LL)=SIN(A)*J0(B)*B
DBOW(LL)=((COS(A)*BESS1(B)*B)*DADW +SIN(A)*(BESS0(B)-BESS1(B))*
9 DBOW(LL))*0.001*3.14159
C PRINT 100,LL,A,B,PHASE(LL),X,INTENS(LL)
100 FORMAT(2X,13,8E14,5)
RETURN
END
FUNCTION BESS0(Z)
DIMENSION X(22),Y(22)
Y(1)=1.
Y(2)=.9975
Y(3)=.99
Y(4)=.9776
Y(5)=.9604
Y(6)=.9385
Y(7)=.9120
Y(8)=.8812
Y(9)=.8463
Y(10)=.8075
Y(11)=.7652
Y(12)=.7196
Y(13)=.6711
Y(14)=.6201
Y(15)=.5669
Y(16)=.5118
Y(17)=.4554
Y(18)=.3980
Y(19)=.3400
Y(20)=.2818
Y(21)=.2239
Y(22)=.1666
X(1) = 0.
X(2) = 0.1
X(3) = 0.2
X(4) = 0.3
X(5) = 0.4
X(6) = 0.5
X(7) = 0.6
X(8) = 0.7
X(9) = 0.8
X(10)= .9
X(11)=1.0
X(12)=1.1
X(13)=1.2
X(14)=1.3
X(15)=1.4
X(16)=1.5
X(17)=1.6
X(18)=1.7
X(19)=1.8
X(20)=1.9

```

```

X(21)=2.0
X(22)=2.1
IL=1
DO 1 I=1,21
  IF(X(I) .LT. Z) IL=I
1  CONTINUE
  BESS0 =Y(IL)+(Y(IL+1)-Y(IL))*(Z-X(IL))/(X(IL+1)-X(IL))
  RETURN
END
FUNCTION BESS1(Z)
  DIMENSION X(22),Y(22)
  IF(Z .EQ. 0.)GO TO 10
  GO TO 11
10  BESS1 = .5
  GO TO 12
11  CONTINUE
  Y(1) = 0.
  Y(2) = .005
  Y(3) = .0198
  Y(4) = .0438
  Y(5) = .0763
  Y(6) = .1166
  Y(7) = .1619
  Y(8) = .2119
  Y(9) = .2646
  Y(10) = .3179
  Y(11) = .3703
  Y(12) = .4197
  Y(13) = .4644
  Y(14) = .5030
  Y(15) = .5340
  Y(16) = .5538
  Y(17) = .5663
  Y(18) = .5697
  Y(19) = .5730
  Y(20) = .5663
  Y(21) = .5500
  Y(22) = .5244
  X(1) = 0.0
  X(2) = .1
  X(3) = .2
  X(4) = .3
  X(5) = .4
  X(6) = .5
  X(7) = .6
  X(8) = .7
  X(9) = .8
  X(10) = .9
  X(11) = 1.0
  X(12) = 1.1
  X(13) = 1.2
  X(14) = 1.3
  X(15) = 1.4
  X(16) = 1.5
  X(17) = 1.57
  X(18) = 1.6
  X(19) = 1.7
  X(20) = 1.8
  X(21) = 1.9
  X(22) = 2.0
  IL = 1
  DO 1 I=1,21

```

```

      IF (X(I)) .LT. ZPTL = 1
1  CONTINUE
      HESS1=Y(IL)+(Y(IL+1)-Y(IL))*(Z-X(IL))/(X(IL+1)-X(IL))
      HFSS1=HFSS1/Z
12 CONTINUE
      RETURN
      END
      SUBROUTINE KERRPL(IMAX,KK,NN)
      IMAX IS NO. OF INPUT POINTS,KK=0 PRINTS VARIABLES,IMAX/NN IS NO. OF POINT
      S PLOTTED.
      DIMENSION DBDW(600),PHASE(600),INTENS(600),FREQ(600),C(10),TAU(10)
      DIMENSION AMP(600)
      COMMON AMP,PHASE,INTENS,FREQ,C,TAU,DBDW
      DIMENSION LINE(115)
      DATA (BLANK=1H ),(DOT=1H.), (STAR=1H*), (XPT=1HX), (YPT=1HY), (ZPT=1HZ)
      REAL INTENS
      INTEGER BLANK,DOT,STAR,XPT,YPT,ZPT
      IF (IMAX) 2,1,2
1  IMAX = 50
2  CONTINUE
      IF (KK) 10,11,10
11 PRINT 100
100 FORMAT(1H1,20X,9HAMPLITUDE,11X,10HDERIVATIVE,10X,5HPHASE,15X,
9 9HINTENSITY,11X,9HFREQUENCY)
      PRINT 101,(I,AMP(I),DBDW(I),PHASE(I),INTENS(I),FREQ(I),I=1,IMAX,
9  NN)
101 FORMAT(1H ,5X,15,5E20.5)
10 PHMAX = ABS(PHASE(1))
      AMPMAX = ABS(AMP(1))
      RNTMAX = ABS(INTENS(1))
      DBDMAX=ABS(DBDW(1))
      DO 3 I=2,IMAX
      IF(DBDMAX .LT. ABS(DBDW(I)))DBDMAX=ABS(DBDW(I))
      IF(AMPMAX .LT. ABS(AMP(I)))AMPMAX = ABS(AMP(I))
      IF (PHMAX .LT. ABS(PHASE(I)))PHMAX = ABS(PHASE(I))
      IF (RNTMAX .LT. ABS(INTENS(I)))RNTMAX = ABS(INTENS(I))
3  CONTINUE
      PRINT 107
107 FORMAT(1H1,11X,17HMAXIMUM AMPLITUDE,3X,18HMAXIMUM DERIVATIVE,
9 2X,13HMAXIMUM PHASE,7X,17HMAXIMUM INTENSITY)
      PRINT 102,AMPMAX,DBDMAX,PHMAX,RNTMAX
102 FORMAT(11X,4E20.6)
      DO 7 J=1,115
7  LINE(J) = DOT
      PRINT 103,LINE
103 FORMAT(1H0,115A1)
      DO 20 J=1,115
20  LINE(J) = BLANK
      DO 6 I = 1,IMAX,NN
      LINE(56) = DOT
      K = 55.+55.*AMP(I)/AMPMAX
      L = 55.+55.*PHASE(I)/PHMAX
      M = 55.+55.*INTENS(I)/RNTMAX
      N=55.+55.*DBDW(I)/DBDMAX
      K = K+1
      L=L+1
      M=M+1
      N=N+1
      LINE(K) = STAR
      LINE(L) = XPT
      LINE (M) = YPT
      LINE(N)=ZPT

```

39

APPENDIX VI

DIFFERENTIAL KERR SPECTROMETER

One disadvantage to measuring the Kerr effect directly is that the measuring equipment must have response at the frequency of the applied electric field. At frequencies above 100 kHz, such equipment becomes more specialized and more difficult to obtain. Outlined herein is a scheme which reduces the electronics requirement to measurements at a constant audiofrequency, but which measures the Kerr response curve as a function of the frequency of the applied field.

Recalling the typical Kerr response curve (Fig. 25a), it is of interest to show the function $d|B|/df$ (Fig. 25b). This function peaks at the critical frequency and has a half width which is directly related to the breadth in frequency of the dispersion part of the Kerr response curve. The peak amplitude of the $d|B|/df$

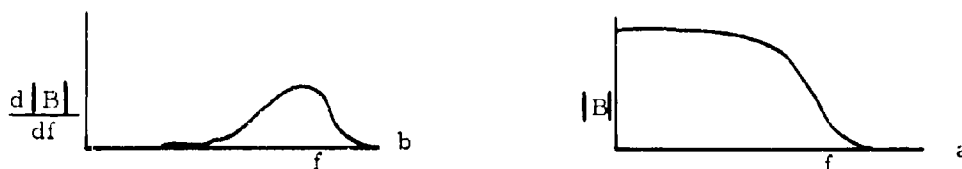


FIGURE 25. KERR RESPONSE CURVE AND ITS DERIVATIVE WITH RESPECT TO FREQUENCY

curve is related through experimental constants to the amplitude of the $|B|$ curve. The area under the $d|B|/df$ curve is a direct measure of the amount of decrease in the $|B|$ curve. That is, an integral of the $d|B|/df$ curve with frequency reproduces the $|B|$ curve when the integration is begun at high frequencies.

The principal advantage to using a device measuring $d|B|/df$ is the simplification of the experimental arrangement. The device could be made as shown in Figure 26.

The feedback is used to drive the power amplifier at the frequency to which the LC circuit is tuned. That is, the system is a self-oscillating one. The capacitor C_1 represents the Kerr cell itself, while C_2 is a

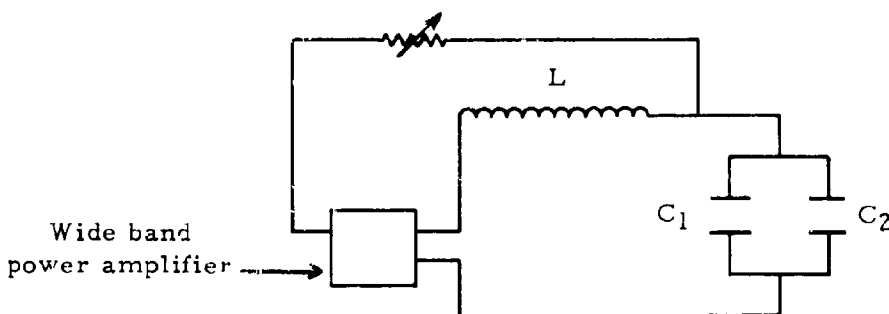


FIGURE 26. BLOCK DIAGRAM OF DIFFERENTIAL KERR SPECTROMETER

time-varying capacitor. The capacitor C_2 may be a motor driven rotating capacitor, or it may be parallel plates mounted on a tuning fork. The analysis of the circuit given below is based upon a tuning fork capacitor. The basic equation is:

$$f = \frac{1}{2\pi \sqrt{LC}} \quad (1)$$

and here

$$C = C_1 + C_2 \quad (2)$$

Based on two parallel plates set a distance d_o apart at equilibrium and having an amplitude of vibration d_1 , C_2 becomes

$$C_2 = \frac{k}{d_o + d_1 \sin \omega t} \quad (3)$$

Substituting for C in Equation (1), we get

$$f = \frac{1}{2\pi \sqrt{L \left(C_1 + \frac{k}{d_o + d_1 \sin \omega t} \right)}} \quad (4)$$

Expanding f in a Taylor's series as a function of $\sin \omega t$, substituting

$$f_o = \frac{1}{2\pi \sqrt{LC_1 + \frac{Lk}{d_o}}}$$

and

$$C_{2o} = \frac{k}{d_o}$$

we get

$$f = f_o - f_o \frac{C_{2o}}{2(C_1 + C_{2o})} \frac{d_1}{d_o} \sin \omega t + \dots \quad (5)$$

All factors in the second term are less than one and indeed should be arranged so that

$$\frac{C_{2o}}{2(C_1 + C_{2o})} \frac{d_1}{d_o} \sim 0.1$$

so that the expansion is a valid one. It shows that the experimental arrangement diagrammed above will have a time-varying frequency centered around the central frequency f_o .

The effect of using this arrangement would be to produce a signal at the detector which is proportional to the rate of change of the Kerr constant over the frequency range scanned. That is, a signal will be produced at the modulation frequency (frequency of the tuning fork) which will be greater at one end of the modulation cycle than at the other. The magnitude of this difference is proportional to the slope of the Kerr response curve at that frequency.

Derivative measurements have been used in magnetic resonance experiments for some time, and have proven useful in that greater resolution is possible than when straight absorption measurements are made. The primary reason for utilizing this scheme is to eliminate the need for phase detection at the rf frequencies. The equipment requirements are reduced to a low frequency phase detector and a wideband power amplifier. The simplification makes possible measurements that would otherwise require much time and effort in construction of suitable equipment.

APPENDIX VII

STUDY OF THE RELAXATION TIME OF THE KERR EFFECT BY ALTERNATING CURRENT*

by H. Benoit

SUMMARY

We have realized an apparatus permitting the measurement with alternating current of the instantaneous value of the birefringence in its phase shift with respect to the applied voltage.

With this apparatus, we have studied a solution of tobacco mosaic virus for the frequencies between 25 and 20,000 cps. This has permitted us to give, for the first time, a verification of the theories of the birefringence in alternating current. We have thus measured the mechanism of orientation and measured the rotational diffusion constant of the virus particles. The value found is in good accord with the values determined by other methods.

Introduction

Numerous authors^(1,2,3) have studied the electric birefringence of colloidal suspensions, with alternating current but the results obtained seem rather contradictory. It is, thus, that one often talks of anomalous birefringence. We have therefore proposed to study this phenomenon in a systematic fashion to determine the laws that permit a final account.

Before describing the apparatus that we have used in the measurement that we have effected, we will review briefly the theoretical results that give, in this case, the application of classical laws of Brownian diffusion. This theory, developed by Tummers⁽⁴⁾ and Gutton⁽⁵⁾, is found exposed in a memoir of Peterlin and Stuart⁽⁶⁾, and it is under the form that these last have given it that we are reviewing the broad outlines.

Theory of the Electric Birefringence in Alternating Fields

Let us consider a medium made up of particles forced by an electric field. One knows that the function of the distribution f of the orientations of the molecules at time t is a solution of the differential equation which expresses the general laws of Brownian movement

$$\nabla^2 f + \frac{1}{kT} \operatorname{div} f \operatorname{grad} w = \frac{1}{D} \frac{\partial f}{\partial t} \quad (1)$$

In this expression, K is the Boltzmann constant, T the absolute temperature, w the energy of the particles at a given instant, and D their rotational diffusion constant, a function of their volume, of their elongment and of the viscosity of the medium.

In order to determine f and, thus, the birefringence of the medium at a time, t , it is necessary to carry in this equation the value of w corresponding to the mechanism of orientation adopted, then to integrate while taking account of the conditions of the problem.

Now, when one knows the molecular theory of the Kerr effect, one sees in general two mechanisms for the orientation of a molecule:

- (1) Orientation by action of a field on a permanent electric moment carried by the molecule.
- (2) Orientation due to the electric anisotropy of the molecule.

*Translated from the French by R. E. Linder.

These two mechanisms coexist in general but, as the term due to the permanent moment is large compared to that of the anisotropy, one can separate the two cases.

For example, if we suppose that the electric field applied to a solution is of the form: $E = E_{ef} \sqrt{2} \cos \omega t$, where $\omega = 2\pi N$, N being the frequency of the alternating field, and we call Δn_o the difference between the indices of the medium in the direction of the applied field and in the direction perpendicular, when it is subjected to a constant field E_{ef} .

In carrying successively in Equation (1) the values of w corresponding to the two mechanisms of orientation envisaged, one can integrate the differential equation and one finds for the birefringence Δn at time t the following expression:

- (1) If the orientation is due to a permanent moment carried by the molecules:

$$\Delta n = \Delta n_o \left[\frac{1}{1 + \frac{9}{4} \omega^2 \tau^2} + \frac{\cos(2\omega t - \delta_2)}{\sqrt{1 + \omega^2 \tau^2} \sqrt{1 + \frac{9}{4} \omega^2 \tau^2}} \right]$$

where $\tau = 1/(3D)$ and where δ_2 is defined by the relation:

$$\tan \delta_2 = \frac{5\omega\tau}{2 - 3\omega^2\tau^2}$$

- (2) If the orientation is uniquely provided by an induced moment, one obtains:

$$\Delta n = \Delta n_o \left[1 + \frac{\cos(2\omega t - \delta_1)}{\sqrt{1 + \omega^2 \tau^2}} \right]$$

δ_1 being defined by the relation: $\tan \delta_1 = \omega\tau$.

One sees that, in these two cases, the birefringence oscillates between the two extreme values that are functions of the frequency of the applied field and which coincide when this frequency is indefinitely increased. In the first case, the birefringence tends toward zero, while, in the second, it tends toward the median value Δn_o . Figures 1 and 2 represent graphically as a function of $\log \omega\tau$ the extreme values of $\Delta n/\Delta n_o$, also the value of δ . Figure 1 in the case of orientation dipole moment. Figure 2 in the case of orientation of an induced moment.

One sees that the aspect of the curves is entirely different and that their experimental determination permits the determination of τ , as well as the rotational diffusion constant of the substance studied.

1. Experimental Apparatus

In order to determine if the theory that we have enunciated applies to the problem that we have posed, it is necessary to measure, as a function of frequency, the maximum birefringence, the minimum birefringence, as well as the phase shift. We have therefore realized an apparatus permitting the determination of these quantities and of which the schematic diagram is represented in Figure 3.

A luminous source (an incandescent lamp) sends a narrow parallel beam to traverse a Kerr cell placed between two crossed Nichols. A signal generator furnishes the sinusoidal voltage which one can vary the frequency. It is followed by an amplifier the output of which is relayed directly to the terminals of the sample cell and to the horizontal deflection plates of an oscilloscope. A photomultiplier p is placed behind the analyzer, it is followed by a large band pass amplifier from 20 cycles to 6 megacycles without phase distortion; the output of this amplifier is relayed to the vertical plates of the oscilloscope. The tube that we have used is a deep tube with a blue spot; it functions with a post-acceleration voltage of 3000 volts, which permits us to photograph the oscillograms easily.

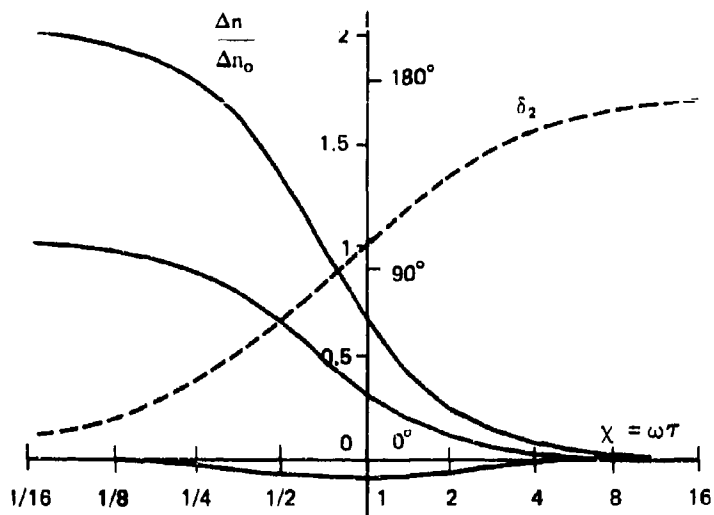


Figure 1. Orientation by a permanent moment.
 Plane curve: maximum birefringence, minimum and median.
 Dotted curve: dephasing between the birefringence and the applied field.
 The abscissa: the frequency of the applied field.

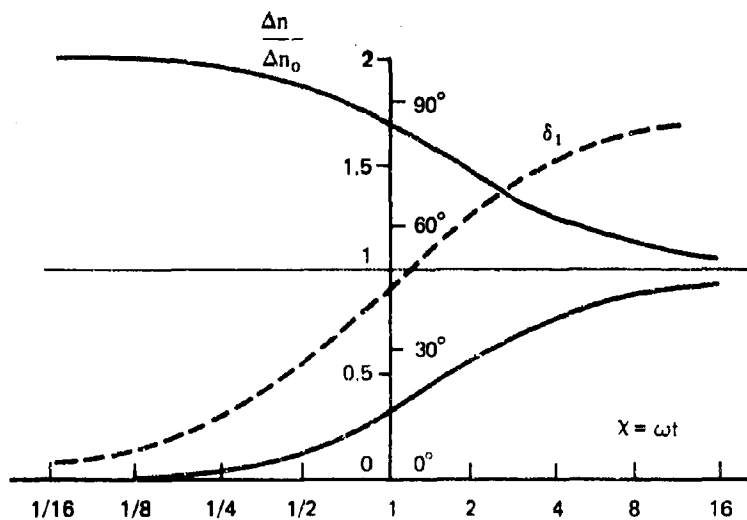


Figure 2. Orientation by induced moment.
 Plain curve: maximum birefringence, minimum and median.
 Dotted curve: dephasing between the birefringence and the applied field.
 The abscissa: frequency of the applied field.

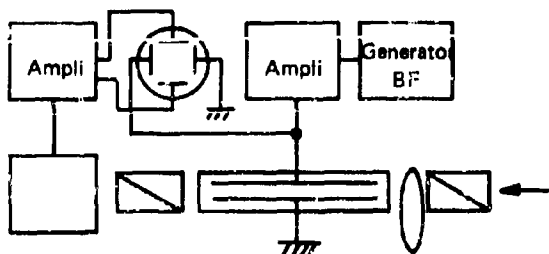


Figure 3. Schematic diagram of the principal parts of the apparatus.



Figure 4. Oscillogram obtained while observing nitrobenzene: frequency 10,000 cycles, the applied voltage 500 volts effective.

Under these conditions, one obtains on the screen of the oscilloscope a curve analogous to the Lissajous curve of order 2, because the light is modulated at a frequency double the frequency of the exciting voltage. In order to deduce from the curves the value of birefringence Δn , it is necessary to know the origin. That is to say, the ordinate on the oscilloscope screen of the trace corresponding to $\Delta n = 0$. For this, we have utilized the following artifice. A turning disc is placed in the path of the luminous beam and interrupts the luminous beam at around 100 times a second. Under these conditions, at the moment when the beam is interrupted, the spot describes a horizontal line which coincides with the line $\Delta n = 0$, if one neglects completely the luminescent parasite due to the fact that the extinction between the crossed Nichols is not total.

Figure 4 shows, for example, the oscillogram obtained in these conditions with nitrobenzene. The applied field has a value of the order of 1500 volts per centimeter and a frequency of 10,000 cps. One sees that the birefringence is annulled at the same time as the voltage, which corresponds very well to theoretical results in the case where the frequency of the electric field is very small compared to the rotational diffusion constant of the substance studied, a constant that is of the order of 10^9 sec.⁽⁷⁾

II. Measurements

We have utilized as a model a suspension of tobacco mosaic virus in distilled water. One knows, on one hand, that these solutions present a considerable Kerr effect, and that, on the other hand, one can measure the dimensions of the particles in an electronic microscope that permits the verification of the experimental results. It is thus that one has utilized these solutions to verify the theories of emission birefringence⁽⁹⁾ of the diffusion of light^(10,11) and of the Kerr effect with rectangular voltage impulses.⁽¹²⁾ All these experiments show that the behavior of these solutions is absolutely normal at weak concentrations; we have, therefore, been content to study two solutions respectively at 10 and 5 mg per 100 cc. The results obtained being, within the error of experiment, identical, and we contented ourselves to reproduce here those which are relative to the first series of experiments. We have made the frequency of the alternating field applied to the cell vary between 20 cycles and 20,000 cycles per second and Figures 5, 6, and 7 show the oscillograms obtained for $N = 50$, $N = 200$, $N = 20,000$. One sees immediately, in a



Figure 5. Birefringence of a solution of tobacco mosaic virus, 10 mg in 100 cc. $N = 50$.



Figure 6. Birefringence of the same solution for $N = 200$.

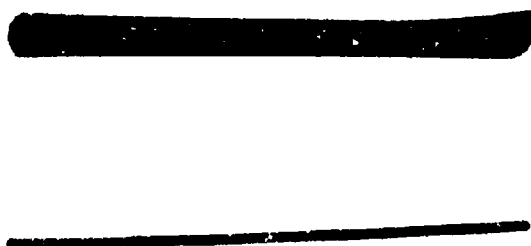


Figure 7. Birefringence of the same solution for $N = 20,000$.

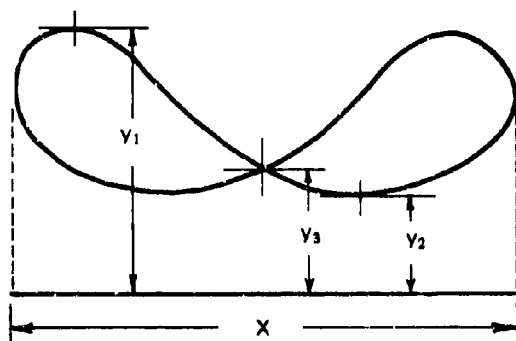


Figure 8

But, in order to trace the curves corresponding to Figures 1 and 2, it is necessary to return for all frequencies to a constant value of the applied electric field. We assume, therefore, that which is experimentally verified, that the birefringence is proportional to the field strength and in calling X the length of the horizontal trace, we can write that the specific birefringence is given by the formulas:

$$\Delta n \text{ max} = K \frac{\sqrt{y_1} y_o}{X^2}$$

$$\Delta n \text{ min} = K \frac{\sqrt{y_2} y_o}{X^2}$$

where K is an arbitrary constant dependent on the calibration of the apparatus. Finally, we obtain the value of the phase shift by the relation

$$\cos \delta = \frac{\sqrt{y_1} y_o + \sqrt{y_2} y_o - 2\sqrt{y_3} y_o}{\sqrt{y_1} y_o - \sqrt{y_2} y_o}$$

Figure 9 represents the experimental results obtained while using as an abscissa the logarithm of the frequency. For high frequencies, the measure of δ becomes difficult and almost impossible, because the differences between y_1 , y_2 , and y_3 are of the same order of magnitude as the noise of the photomultiplier. One sees, also, that with experimental errors, the experimental results are well grouped on the curve having the same aspect as those that permit the calculation of the theory in the case of orientation by induced moment. From these curves, one can obtain the value of rotational diffusion constant by two methods:

quantitative fashion, that the phase shift between the applied voltage and the observed birefringence takes considerable values and that when the frequency increases the birefringence remains constant and different from 0. This led us to the conclusion that the orientation couple is of the type by induced moment and not by permanent moment which verifies the result that we have obtained in studying the Kerr effect of these solutions by another method.⁽¹²⁾

In order to verify the theory in a more quantitative fashion, it was necessary for us to trace for a constant value of E_{ef} the curves $\Delta n \text{ max}$, $\Delta n \text{ min}$, and δ as a function of the frequency. For this, we measured on a large plate the known relationship between the three quantities y_1 , y_2 , y_3 corresponding to the ordinate of the highest point, the lowest point, and the point of intersection of the two parts of the Lissajous curve (Fig. 8). On the other hand, one can measure while making the turning disc turn in the absence of an electric field the vertical displacement y_o due to the passage of the luminous parasite when the Nichols are crossed. As the birefringences are weak, one can assume⁽¹²⁾ that the birefringence at time t is proportional to the quantity $(y - y_o)^{1/2}$.

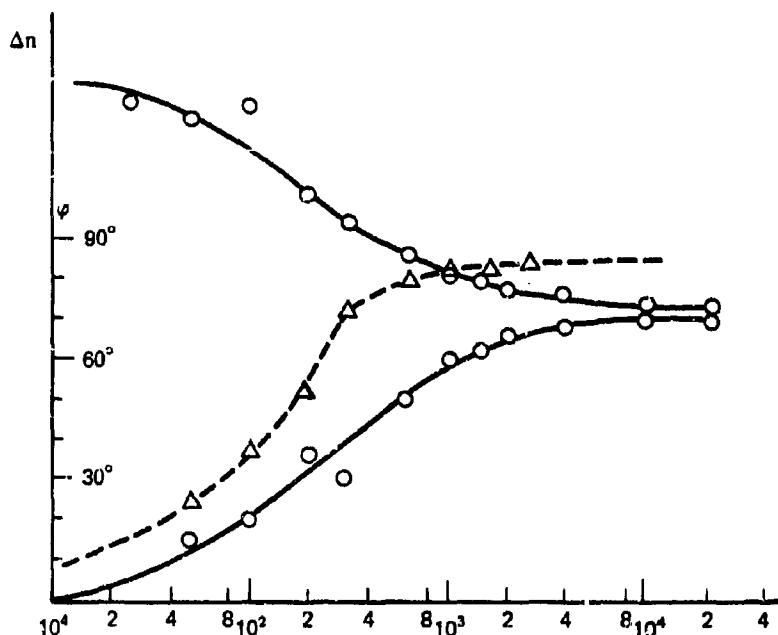


Figure 9. Experimental Results. Solution of tobacco mosaic virus 10 mg per 100 cc. Abscissa: the frequency. Plain curve: maximum and minimum birefringence. Dotted curve: phase shift between the birefringence and the voltage.

- (1) In finding the frequency N_1 , at which $\delta = 45^\circ$;
- (2) In finding the frequency N_2 , for which the curve Δn max or Δn min presents a point of inflection.

These two frequencies N_1 and N_2 are related to the rotational diffusion constant of the median assumed monodisperse by the relations:

$$N_1 = \frac{3}{2\pi} D$$

$$N_2 = \frac{3\sqrt{2}}{2\pi} D$$

which permit, knowing N_1 and N_2 , the calculation of D . According to whether one utilizes the first or the second method, one finds:

$$D_1 = 320 \text{ sec}^{-1} \quad D_2 = 440 \text{ sec}^{-1}$$

These values are compatible with the results obtained by other methods on suspensions of the same type. In fact, we have found by the Kerr effect study with rectangular impulses, the median value $D = 450 \text{ sec}^{-1}$, but it is evident that these two methods of analysis do not give the same result. In fact, the theoretical curves reproduced in Figures 1 and 2 are relative to a median containing only one species of the molecule. Thus, we have to deal with a mixture of particles of different lengths, that is to say, a polydisperse medium and, in order to have theoretical representation correct to the experimental results, it is necessary to take into

account these phenomena. The formulas are easy to establish; if we call Δn_i and τ_i the birefringence relaxation time corresponding to the species i , one sees that the frequency ω for which $\delta = 45^\circ$ is a root of the equation:

$$\sum n_i (1 + \omega^2 \tau_i^2)^{-1/2} (2 \cos \delta_i - \sqrt{2}) = 0$$

where δ is defined by the relation $\tan \delta_i = 1/(\omega \tau_i)$, the summation extends over all species of molecules presented in the solution. On the other hand, the frequency ω for which the curves Δn max and Δn min present an inflection point, would be roots of the equation:

$$\sum \Delta n_i (1 + \omega^2 \tau_i^2)^{-5/2} (2 - \omega^2 \tau_i^2) = 0 \text{ with } \tau_i = \frac{1}{3D}$$

D_i being the rotational diffusion constant for the species i . This shows well that the median values measured by the two methods have no reason to be equal. But one also sees that these equations are rather difficult to manage, seeing the presence of the radicals, which leads us to the conclusions that the study of the polydispersity by this method will be more complicated than by the rectangular impulse method.

In summary, we have shown that the laws of dispersion of the Kerr effect as a function of the frequency of applied field as applied to suspensions of tobacco mosaic virus. With this, we have shown the mechanism of orientation as well as given a value approaching the rotational diffusion constant of these molecules in suspension. In spite of these results, this method seems difficult to apply to the case of polydispersed media because it is less precise and less easy to utilize than the method of rectangular impulses.

APPENDIX VII

REFERENCES

1. J. Rabinovitch, *J. Phys. et le Radium* (1946) 7, 228.
2. W. Heller, *Review of Modern Phys.* (1942), 14, 390.
3. B. Muller, B. W. Sackmann, *Phys. Rev.*, 56 (1939), 615.
H. Muller, *Phys. Rev.* (1939), 55, 792.
4. J. H. Tummers, *Diss. Utrecht*, 1914.
5. C. Gutton, *J. Phys. et le Radium* (1906), 5, 213.
6. A. Peterlin et H. A. Stuart, *Hand und Jahrbuch der Chem. Physik*, 8, 1 B.
7. O. Maerks et W. Hanle, *Phys. Z.* (1938), 39, 852; *Z. für Phys.* (1939), 114, 407.
8. M. A. Lauffer, *J. Am. Chem. Soc.* (1939), 61, 2412.
9. J. B. Donnet, *C. R.* (1949), 229, 189.
10. G. Oster, P. M. Doty et B. H. Zimm, *J. Am. Chem. Soc.* (1947), C9, 1193.
11. P. Horn, *C. R.*, 234 (1952), 1870.
12. H. Benoit, *Ann. de Physique* (1951), 12^e série, 6, 561.

APPENDIX VIII

BIBLIOGRAPHY

- Benoit, H., "Contribution to the Study of the Kerr Effect from Dilute Solutions of Rigid Macromolecules," *Ann de Phys*, **6**, 1951, 36.
- Benoit, H., "Study of the Relaxation Times of the Kerr Effect by Alternating Current," *J Chim Phys*, **49**, 1952, 58.
- Benoit, H., Freund, L., and Spach, A., "Dilute Solution of Polypeptides: Light Scattering and Hydrodynamics," *Poly- α -Amino Acids*, ed G. Fasman, Marcel Dekker, New York, 1967, 105.
- Boeckel, G., Genzling, J., Weill, G., and Benoit, H., "Study of the Kerr Effect of the Poly Benzyl-L-Glutamate in Solution," *J Chim Phys*, **59** 1962, 999.
- Buckingham, A.D., "Frequency Dependence of the Kerr Constant," *Proc Roy Soc, A*, **267**, 1962, 1328.
- Buckingham, A.D., and On, B.J., "Kerr Effect in Methane and Its Four Fluorinated Derivatives," *Trans Far Soc*, 1969, 673.
- Buckingham, A.D. and On, B.J., "Molecular Hyperpolarizabilities," *Quarterly Reviews*, **21**, 1967, 195.
- Czehalla, J. and Wick, G., "Determination of Absolute Transition Moment Directions and of Dipole Moments of Excited Molecules from Measurements of the Electric Dichroism," *Zeitschrift F. Elektrochemie*, **65**, 1961, 727.
- Debye, P., "The Theory of Anomalous Dispersion in the Region of Long-Wave Electromagnetic Radiation," *Berichte Gesellschaft*, **15**, 1913, 777.
- Dow, D.A., "Kerr Effect in Flexible Polymers," *J Chem Phys*, **41**, No. 9, 1964, 2656-2660.
- Heller, W., "The Origin and the Complications of Electric Double Refraction and of Electric Dichroism in Dilute Dispersed Systems," *Reviews of Modern Physics*, **14**, No. 4, 1942, 390.
- Jennings, B.R. and Jenard, H.G., "Light Scattering by Poly- γ -Benzyl-L-Glutamate Solutions Subjected to Electric Fields," *J Phys Chem*, **69**, 1965, 2817.
- Krause, S. and O'Konski, C.T., "Electric Properties of Macromolecules. III. Kerr Constants and Rotational Diffusion of Bovine Serum Albumin in Aqueous Solutions," *J Am Chem Soc*, **81**, 1959, 5082.
- Labhart, H., "Electrochromism," *Advances in Chemical Physics*, Vol. XIII, ed I. Prigogine, Interscience, New York, 179.
- Labhart, H., "Survey of the Method for the Determination of Charge Distribution in Electronically Excited Molecules," *Experientia*, **22**, 1966, 65.
- Lin, S.H., Lin, C.Y., and Eyring, H., "The Dispersion of Electric Birefringence," *J Phys Chem*, **70**, 1966, 1756.
- Marchal, E., Hormick, C., and Benoit, H., "Study of Two Species of Poly-Benzyl- α -L-Glutamate by Dielectric Absorption and Kerr Effect in Dilute Solution in 1-2 Dichlorethane," *J Chim Phys*, **64**, 1967, 575.

- Marchal, E., Marchal, I., and Benoit, H., "Principles of Calculating the Molecular Weight Distribution Curve Using Dipole Absorption Spectra Due to Orientation of Macromolecules in Dilute Solution," *J Chim Phys*, **63**, 1966, 1247.
- O'Konski, C.T. and Haltner, A.J., "Characterization of the Monomer and Dimer of Tobacco Mosaic Virus by Transient Electric Birefringence," *J Am Chem Soc*, **78**, 1956, 3604.
- O'Konski, C.T. and Haltner, A.J., "Electric Properties of Macromolecules. I. A Study of Electric Polarization in Polyelectrolyte Solutions by Means of Electric Birefringence," *J Am Chem Soc*, **79**, 1957, 5634.
- O'Konski, C.T. and Zimm, B.H., "New Method for Studying Electrical Orientation and Relaxation Effects in Aqueous Colloids: Preliminary Results with Tobacco Mosaic Virus," *Science*, **111**, 1950, 113.
- O'Konski, C.T., Yoshioka, Koshiro, and Orttung, W.H., "Electric Properties of Macromolecules. IV. Determination of Electric and Optical Parameters from Saturation of Electric Birefringence in Solutions," *J Phys Chem*, **63**, 1959, 1558.
- Shah, M.J., "Electric Birefringence of Bentonite. II. An Extension of Saturation Birefringence Theory," *J Phys Chem*, **67**, 1963, 2215.
- Shah, M.J. and Hart, C.M., "Investigations of the Electro-Optical Birefringence of Polydisperse Bentonite Suspensions," *IBM Journal*, **7**, No. 1, 1963, 44.
- Tinoco, I., Jr., "Dynamic Electrical Birefringence Studies of Poly- γ -benzyl-L-glutamate," *J Am Chem Soc*, **79**, 1957, 4336.
- Wada, A., "Dielectric Properties of Polypeptides," *Poly- α -Amino Acids*, ed G. D. Fasman, Marcel Dekker, New York, 1967, 369.
- Wada, A., "Dielectric Properties of Polypeptide Solutions, II," *J Chem Phys*, **30**, 1959, 328.
- Wallach, M.L. and Benoit, H., "Light Scattering by Poly-L-Benzyl Glutamate Solutions Subjected to an Electrical Field," *J Poly Sci*, **57**, 1962, 41.
- Watanabe, H., Yoshioka, K., and Wada, A., "Electro-Optical and Dielectric Investigations on the Conformation and the Electrical Properties of Poly- γ -Benzyl-L-Glutamate in Mixed Solvents," *Biopolymers*, **2**, 1964, 91.
- Weber, G., "Polarization of the Fluorescence of Solutions Subjected to an Electric Field," *J Chem Phys*, **43**, 1965, 521.

UNCLASSIFIED

Security Classification

DOCUMENT CONTROL DATA - R & D

(Security classification of title, body of abstract and indexing annotation must be entered when the overall report is classified)

1. ORIGINATING ACTIVITY (Corporate author) Southwest Research Institute 8500 Culebra Road San Antonio, Texas 78228		2a. REPORT SECURITY CLASSIFICATION UNCLASSIFIED	
		2b. GROUP	
3. REPORT TITLE PRELIMINARY EVALUATION OF THE KERR EFFECT PHASE SHIFT AS A TECHNIQUE FOR CHEMICAL ANALYSIS			
4. DESCRIPTIVE NOTES (Type of report and inclusive dates) Technical Report, 2 December 1968 through 1 November 1969			
5. AUTHOR(S) (First name, middle initial, last name) John R. Rowlands Robert E. Linder Eugene T. Krasicki			
6. REPORT DATE March 1970		7a. TOTAL NO. OF PAGES 52 pp. & Preliminaries	7b. NO. OF REFS 42
8a. CONTRACT OR GRANT NO. F33615-69-C-1231		9a. ORIGINATOR'S REPORT NUMBER(S) RS-536	
b. PROJECT NO. 3048		9b. OTHER REPORT NO(S) (Any other numbers that may be assigned this report)	
c.		AFAPL-TR-70-4	
d.			
10. DISTRIBUTION STATEMENT This document has been approved for public release and sale, its distribution is unlimited.			
11. SUPPLEMENTARY NOTES		12. SPONSORING MILITARY ACTIVITY Air Force Aero Propulsion Laboratory Air Force Systems Command Wright-Patterson Air Force Base, Ohio	
13. ABSTRACT Several optical techniques are of interest as possible approaches to the chemical analysis of fuels and lubricants. Of these techniques, measurement of the phase shift or time lag in the Kerr effect was chosen for initial investigation. A breadboard device was constructed to measure the phase shift at frequencies from 200 Hz to 100 kHz. This device was used to measure the critical frequencies of poly- γ -benzyl-L-glutamate (1500 Hz), Acryloid HF-866 (1900 Hz), a probable impurity in lubricant ester S-9 (1000 Hz), and lubricant ester S-7 (>5 kHz), and also to analyze quantitatively a mixture of Acryloid HF-866 and the impure ester S-9. A spectrometer of simpler construction than the current instrument was designed to facilitate extending the measurements to higher frequencies on the order of 1 MHz, so that a wider range of molecular sizes and structures can be investigated. Also, the equations describing the Kerr response curve of mixtures were derived. Some numerical tests of the simple analysis procedures were compared with the results of these equations, and intensity and derivative spectra for representative mixtures were obtained.			

END

DD FORM 1 NOV 65 1473

UNCLASSIFIED

Security Classification